DNA Walkers: Emerging Analytical Applications, Biomolecular-Nanomaterial Probes and Biomolecule Sensors

Sean Mason

A Thesis Submitted to the Department of Chemistry

In Partial Fulfillment of the Requirements for the

Degree of Master of Science

Brock University

St. Catharines, Ontario

Abstract

DNA walkers are a unique class of dynamic DNA devices that move nucleic acid walkers processively along designated one-, two-, or three-dimensional tracks. Because of the unique mechanical motion, dynamic interaction, and capabilities for signal amplification, programmable signal transduction, high directionality, and predictable analytical performance on the basis of Watson-Crick base paring rules, this class of dynamic DNA nanodevice has gained great attention from the analytical community in the recent years. This includes bioanalytical applications that range from nucleic acid sensing, to protein detection and to cellular imaging and analysis. The research described herein focuses on improving the understanding of biophysical processes involved in the design and operation of DNA walkers. Specifically, we developed a series of stochastic DNA walkers capable of probing dynamic interactions occurring at the biomolecule-nanoparticle (bio-nano) interface. By monitoring dynamics of DNA walkers on spherical nucleic acid (SNA) tracks, we systematically investigated effects of varying interfacial factors, including intramolecular interactions, orientation, cooperativity, steric effect, multivalence, and binding hindrance on enzymatic activities at the bio-nano interface. Leveraging the newly gained knowledge at the interface, we also fabricated ultrasensitive biosensors for amplified detection of nucleic acids and antibodies. Our study revealed critical roles of interfacial factors to enzyme activities and performance of enzyme-driven nanodevices. We also demonstrate that improvement in understanding bio-nano interfaces will facilitate the design and operation of biosensors and inspire new sensing mechanisms.

Acknowledgments

I would like to thank my research supervisor and mentor for the last four years of my life, Dr. Feng Li, for introducing me and accepting me into his group, as well as providing me with guidance and leadership which helped me to achieve my research goals. I would also like to thank my supervisors, Dr. Heather Gordon, as well as Dr. Tony Yan, for the support and suggestions in my research and writing. I would like to thank the members of the Li group, past and present. Thank you for the research suggestions and all the time we've spent together. I would also like to thank Xaiolong Yang for teaching me everything I know within the lab, as well as answering all of my questions, and for all the good times we shared.

To all of my friends at Brock, thank you for always having my back during our time together at school, long or short. Without you, I wouldn't have made it as far as I am today. To the friends outside of school, much of the same. Memories we have made will last a lifetime. Finally, I would like to specially thank both my loving girlfriend, Justine Dyck, and my family, including my brother, sister, mom and dad.

Table of Contents

List of Tables

List of Figures

List of Schemes

List of Abbreviations

DNA	Deoxyribonucleic Acid
RNA	Ribonucleic Acid
A	Adenine
G	Guanine
C	Cytosine
T	Thymine
U	Uracil
1-D	One Dimensional
2-D	Two Dimensional
3-D	Three Dimensional
HCR	Hybridization Chain Reaction
CHA	Catalytic Hairpin Assembly
TMSD	Toehold-Mediated Strand Displacement
ssDNA	Single-stranded DNA
TX	Triplex Crossover DNA
miRNA	MicroRNA
AuNP	Gold Nanoparticle

ECL	Electrochemiluminescence
RCA	Rolling Circle Amplification
FAM	Fluorescin amidite
NP	Nanoparticle
SNA	Spherical Nucleic Acid
BDW	Bipedal DNA Walker
F-Track	20nM AuNP functionalized with FMA labeled oligonucleotides
TAMRA	5- carboxytetramethylrhodamine
T-Track	20nM AuNP functionalized with TAMRA labeled oligonucleotides
PolyA	poly adenine
PolyT	poly thymine
TDW	Tethered DNA Walker
3'SDW	3' single foot DNA walker
5'SDW	5' single foot DNA walker
T	Target
F	Fuel
W1	Waste

DTT	Dithiothreitol
NEBuffer	Nicking Enzyme Buffer
N. Bbv C IB	Nicking Endonuclease

Chapter 1

Emerging Bioanalytical Applications of DNA Walkers

1.1 Introduction

The importance of DNA in living systems is undisputedly known. In eukaryotes, DNA is found in the chromosomes that are located in the nucleus of each cell. These chromosomes contain all the genetic information of the organism, and therefore genes[1]. DNA encoded in genes provides cells with instruction codes to make proteins. The creation of proteins starting with DNA involves an intermediate process involving a second type of nucleic acid, ribonucleic acid (RNA). RNA plays critical biological roles in process such as regulation, expression, coding and decoding of genes.[2]

In 1953, Rosalind Franklin and Maurice Wilkins used X-Ray crystallography to show that DNA had a repetitive helical structure.[3] In the same year, James Watson and Francis Crick proposed the structure of DNA.[1] They proposed that DNA exists in a coiled duplex, held together by hydrogen bonds between the nitrogenous bases.[1] The four heterocyclic bases present in DNA are adenine (A), guanine (G), cytosine (C), and thymine (T). Uracil (U) is a fifth naturally existing base, however it is observed almost exclusively in RNA. The five DNA/ RNA bases are shown in Figure 1.

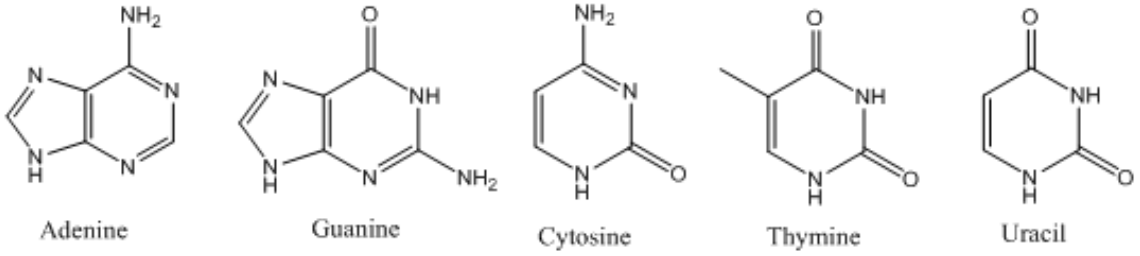

Figure 1: Chemical structure of five bases present in DNA and RNA.

Each nucleotide within a stand of DNA contains one base, which is bound to 2-deoxy-D-ribose, (the sugar), and a phosphate group. The phosphate group links two successive nucleotides together via a phosphodiester bond at the 5' and 3' ends of the nucleotides.[4] The double strand of DNA is then formed between two perfectly complementary strands, in an anti-parallel fashion.

Adenine and guanine are purines, while cytosine, thymine and uracil are pyrimidine bases. Watson and Crick proposed that the hydrogen bonds that hold a DNA duplex together occur only between a pyrine and pyrimidine, due to steric considerations. Therefore, the only possible matching pairs of bases are adenine and thymine (A:T), as well as cytosine and guanine (C:G). There are two hydrogen bonds between adenine and thymine, while cytosine and guanine are held together by three hydrogen bonds (Figure 2). This hydrogen bond arrangement is made under the assumption the bases exist predominately in their keto form.[1]

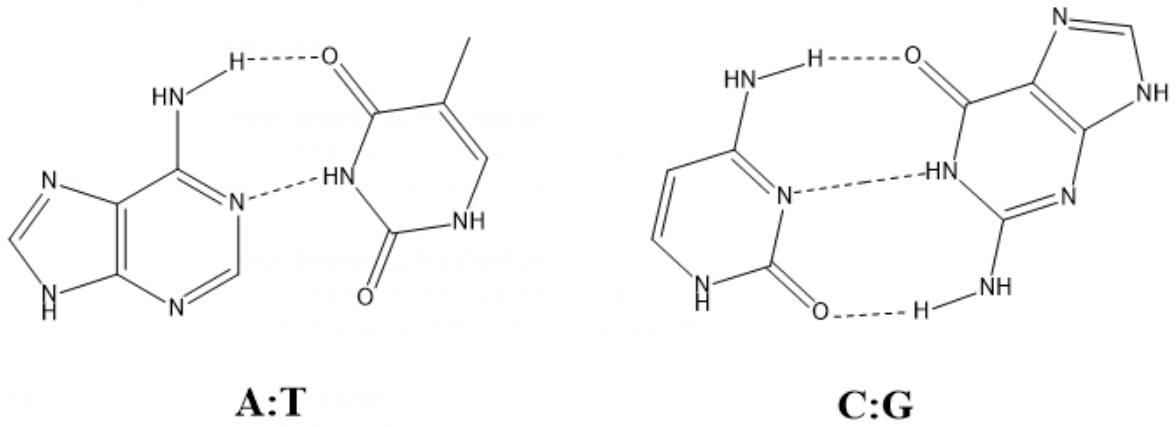

Figure 2: Schematic representation of the base pairing that occurs in double-stranded DNA. Dashed lines represent hydrogen bonding between atoms.

The predictable and robust Watson-Crick base pairing rule makes DNA a suitable material to precisely design nanostructures such as DNA origami and nanodevices, such as DNA walkers. The function of DNA in programming essential components in cells, make the sequence of DNA applicable to the area of disease diagnosis.[5]

This chapter highlights the use of DNA to perform DNA-reactions such as toehold-mediated strand displacement reactions. These DNA- based reactions form the backbone of the design of DNA nanodevices, such as DNA walkers, which have recently been shown to provide avenues for biosensor development for the detection of nucleic acid and proteins, as well as cellular imaging platforms. This chapter has been modified from our recent publication in the journal Trends in Analytical Chemistry.[6]

1.2 DNA Nanotechnology

As an important branch of the field of nanoscience and nanotechnology, DNA nanotechnology has made ever increasing impact in the field of analytical chemistry in recent years.[7-9] Because of

the great structural and functional programmability of Watson-Crick base pairing, DNA can be designed precisely into nanoscale sensors and devices responsive to specific biomolecules, offering remarkable high sensitivity, specificity, robustness and predictability.[8,9] Many concepts and strategies in DNA nanotechnology, such as reconfigurable nanostructures,[10] nanomachines,[11] circuits,[12] and switches,[13] have now been widely adopted for developing promising analytical tools for the detection, quantification, and imaging of biomolecules *in vitro* and *in vivo*. For example, catalytic DNA circuits, such as hybridization chain reactions (HCR),[14] catalytic hairpin assembly (CHA),[15] and entropy-driven DNA catalysis,[16] have enabled diverse isothermal and enzyme-free nucleic acid amplification approaches.[12]

1.2.1 Toehold-Mediated Strand Displacement DNA Reactions

Toehold-mediated strand displacement (TMSD) reactions are simple DNA reactions that can have a very important function in many different systems. In a TMSD reaction, a DNA duplex can be described as having an output strand and a substrate strand. On the substrate strand exists a single-stranded region of 4-10 nucleotides in length,[17] extended from the duplex. This is known as the toehold region. An invading single-stranded (ssDNA) defined as an input strand can bind to the toehold on the substrate strand, and through a process known as branch migration, the substrate strand and input strand will become hybridized, leaving the output strand single-stranded.[17] The length of the branch migration strand should be relatively long (~20nt).[17] The process is energetically favorable due to the longer length of the fully complementary region between the substrate strand and the input strand. A simple model of toehold-mediated strand displacement is outlined in Figure 3.

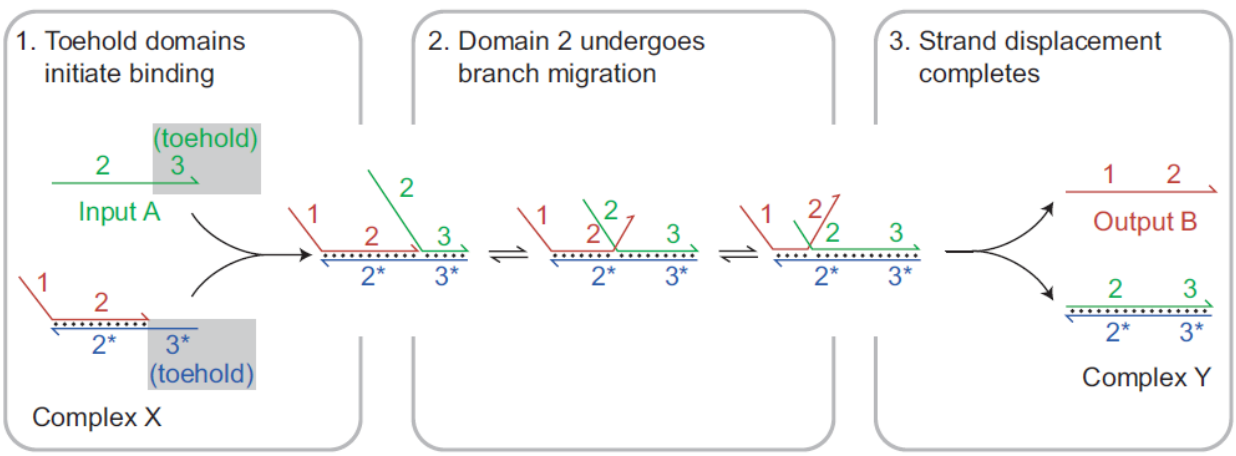

Figure 3: Example of a classic Toehold-mediated Strand Displacement reaction. Modified from Ref. 8. Input A strand (green) represents the input; Complex X contains the output-substrate duplex (output= red, substrate= blue) (section 1). Toehold 3* on the substrate strand contains a region complementary to that on the input strand (3), which initiates input-substrate binding. Branch migration (section 2) displaces the output strand B, leaving the fully complementary input-substrate product (Complex Y) (section 3).

TMSD reactions are used in dynamic DNA nanotechnology. Examples include catalytic DNA circuits, DNA nanomachines, molecular translators, or reconfigurable nanostructures.[17,18] These systems are powerful and robust, given that they are driven by Watson-Crick base-pairing and have the ability to operate without the use of enzymes.[17] The reason that nucleic acids are successful in engineering materials, such as DNA circuits and nanomachines, is due to the predictability and stability of the Watson-Crick base pairs and binding thermodynamics of the walker and track.[16,19]

The design of toehold-exchange mechanisms has promoted the development of DNA probes capable of ultra specific conditional discrimination of DNA sequences with single nucleotide

variations.[19-21] DNA-mediated molecular translators have enabled the amplified detection of non-nucleic-acid targets in homogeneous solutions.[18,23-26]

1.3 DNA Walkers

DNA walkers are the synthetic mimics of naturally occurring molecular walkers, such as dynein, myosin and kinesin, where this nucleic acid mimic is able to move processively along a well-designed track assembled partially or entirely from DNA building blocks.[27-29] Structurally, a DNA walker consists of three essential components, including a walker, a track, and fuel molecules or other forms of energy input that drive the motion. DNA walkers are also characterized fundamentally by their dynamic interactions with the substrate.[27] To be defined as a DNA walker, one of the most important characteristic is the processivity: the ability of a walker molecule to migrate along the track with more than one mechanical cycle.[28] It is also critical that the walker can be reset at the end of each mechanical cycle without undoing the physical task that was originally performed. Directionality towards one end of the DNA track is another important character defining most one-dimensional (1D) DNA walkers. However, for DNA walkers moving on 2D or 3D tracks, the migration can be random, as long as the walker is not detached from the track. Such walkers are generally known as stochastic DNA walkers. An ideal DNA walker should also be autonomous with no human intervention during the operation, but this characteristic is not essential for a functional DNA walker. Nonautonomous DNA walkers are also referred to as DNA steppers.[27] The unique mechanical motion and molecular interactions in DNA walkers can be highly advantageous when applied to developing analytical tools. For example, most DNA walkers are intrinsically signal amplification systems because they will have to repeat mechanical cycles without undoing the previous tasks.[27,28] The directionality of DNA walkers can also be integrated into the development of biosensors for

programming the pathways of signal transduction. The processive motion along a defined track can potentially be harnessed to concentrate the substrates of catalytic reactions or overcome the mass transfer barriers in surface-based sensors, both of which are critical to reduce the sample-to-answer time.[30] In this case, mass transfer barriers refer to a barrier or hindrance to the DNA walker binding to the track, for example viscosity of the solution, which would create a longer time for the binding. A processive walker overcomes a mass transfer barrier because the walker never leaves the track, meaning it never has to diffuse back into solution and bind again to available track strands. In this chapter, the design principles of DNA walkers will first be briefly discussed followed by a focus on their bioanalytical applications.

1.3.1 Design Principles of DNA Walkers

A typical DNA walker consists of three key components, including a walker, a track, and the energy input.[27] The driving forces for most DNA walkers are provided by the hybridization or hydrolysis of the DNA track. Typically, series of toehold-mediated strand displacement reactions are involved to control the direction of movement of DNA walkers.[27-29] For autonomous walking, DNA catalysis mechanisms, such as non-covalent catalysis[31] and catalytic hairpin assembly[32], are typically used to ensure high processivity. Alternatively, 'burnt-bridge' DNA walkers achieve autonomous and directional movements by hydrolyzing the tracks, pushing the walker in the forward direction with the assistance of DNAzyme,[34-36] nicking endonuclease,[37,38] exonuclease,[39] RNase H[40] or light irradiation.[41] To be processive, the walker has to be designed in such a way that the complete detachment from the track is prevented. Therefore, most walkers are bipedal, in that they contain two chemically different feet that bind to an unsymmetrical track (Figure 4a).[42] It is also possible to design DNA walkers with only one foot (inchworm walkers), but a secondary interaction between the foot and the track has to exist to ensure the processivity

(Figure 4b).[34,37] DNA walkers with more than two feet (spider walkers) have also been created, which can migrate with high processivity along their tracks (Figure 4c).[35,36] The track for DNA walkers can be made either partially or entirely of DNA. The first DNA walker introduced by Seeman and Sherman in 2004 was designed to walk along a 1D track made by a triple crossover (TX) DNA with three protruding single strands (Figure 4a).[43]

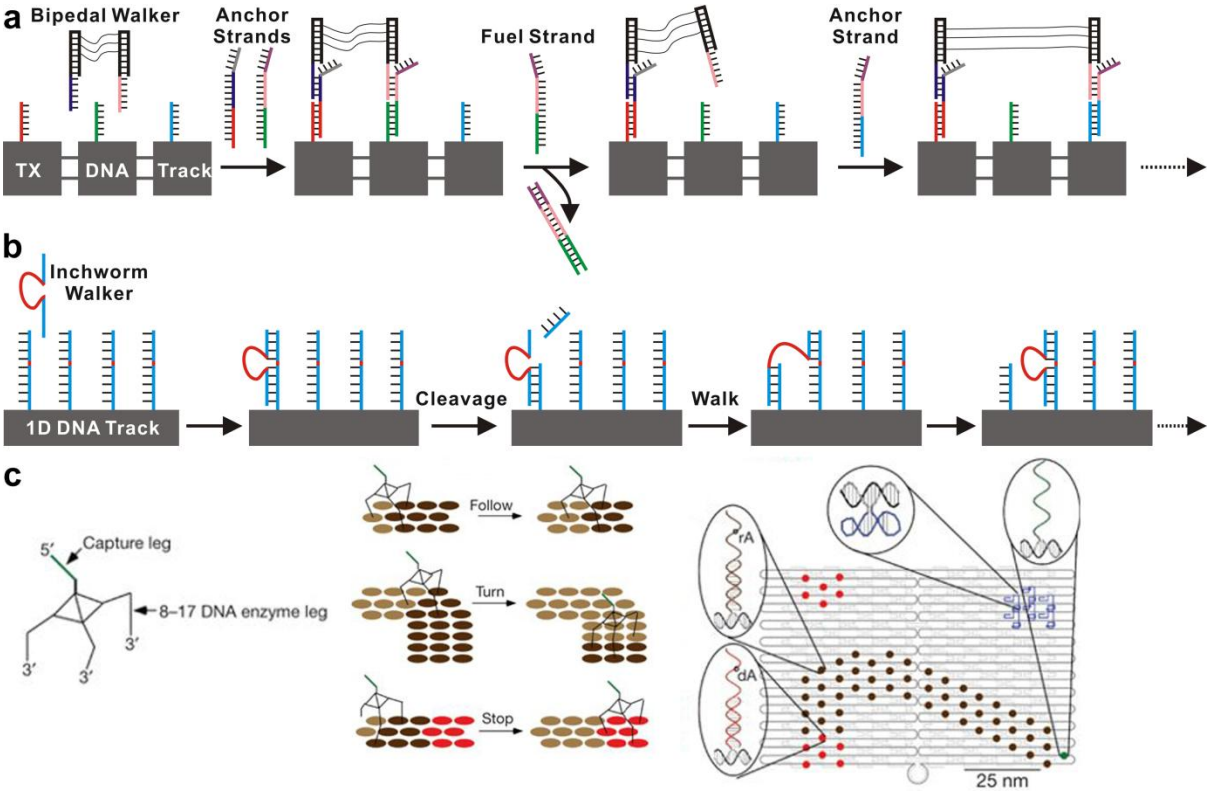

Figure 4. Schematic illustration of representative DNA walkers and track designs. a) A classic bipedal DNA walker travels on a 1D track made of TX DNA. The walking is nonautonomous requiring the addition of fuel strand at each step.[43] b) A burnt-bridge single-foot inchworm DNA walker travels on a 1D DNA track. The walking is driven by the hydrolysis of phosphodiester bonds using a DNAzyme.[33] c) A multi-pedal DNA spider travels on a 2D track made by DNA origami. Driven by the DNAzyme, the DNA spider could autonomously carry out more

sophisticated actions, such as “start”, “follow”, “turn”, and “stop”.[36] Modified with permission from 2010 Springer Nature.

DNA walkers can also move on 2D tracks made of DNA origami, which is a two- or three-dimensional DNA nanostructure made by folding a long single-stranded DNA molecule,[33] or DNA modified planar surfaces. One of the first examples of 2D DNA walkers was the DNA spider that traversed in DNA-modified dextran-streptavidin matrix on a gold substrate.[35] Remarkably, the DNA spider was capable of continuously diffusing through the matrix via biased diffusion and the rate of diffusion could be controlled through variations in recognition regions and the number of feet. When using appropriately designed DNA origami as the 2D track, the same DNA spider could autonomously carry out more sophisticated actions, such as “start”, “follow”, “turn”, and “stop” (Figure 4c).[36] Stochastic DNA walkers traversing on 3D tracks have also been introduced recently.[32,38] DNA functionalized microspheres and nanoparticles are typically used to provide the third plane of directionality. In the following section, DNA walkers will be classified according to the dimensions of their tracks. The analytical applications and/or potential for each class are discussed.

1.4 Bioanalytical Applications of 1D DNA Walkers

Because of the low processivity, 1D DNA walkers have very limited application in bioanalytical techniques due to low signal amplification. However, this class of DNA walkers has the highest level of directionality and controllability, which can be adapted to program signal transduction pathways for biosensors.[43-45] Wang, *et al.* have recently demonstrated that a 1D DNA walker could induce conformational changes of the track in the presence of a target nucleic acids.[43] As shown in Figure 5a, the track was constructed using five oligonucleotides containing three

protruding single-stranded branches separated evenly by the scaffold. In the presence of the let-7a microRNA as the target, the first DNA walker C1 was triggered and moved along the track. The movement of C1 released a second walker C2 moving again along the track. The cascaded walking generated two padlock probes. In the presence of T4 DNA ligase and phi29 polymerase, the two padlock probes were circulated and amplified through rolling circle amplification. Using this DNA walker as a sensor, at concentration as low as 58 fM target miRNA could be detected and be discriminated from other let-7 family miRNAs. In addition to inducing conformational changes, 1D DNA walkers can also be used to control the fluorescence (FRET) or electrochemiluminescence (ECL) energy transfer by precisely tuning the distance between the donors and acceptors through the walking mechanism.[44,45]

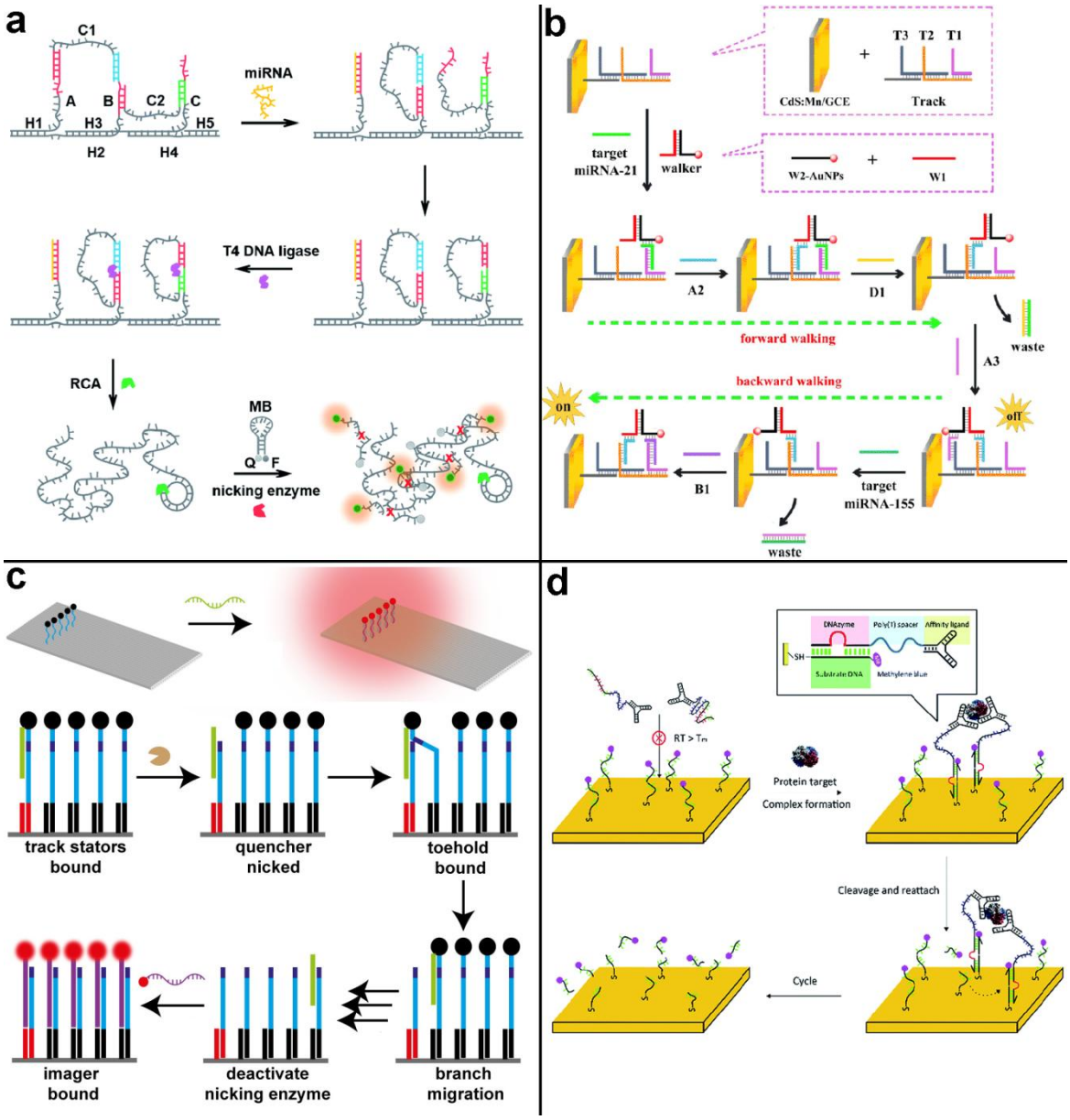

Figure 5. Schematic illustration of 1D and 2D DNA walkers for biomolecular analysis. (a) A 1D DNA walker capable of switching conformations and triggering subsequent rolling circle amplification in response to specific microRNA.[43] Reprinted with permission from 2015 Royal Society of Chemistry. (b) A bidirectional 1D DNA walker that generates detection signals for multiple microRNA targets by controlling the distance-based electrochemiluminescence energy transfer.[44] Reprinted with permission from 2017 American Chemical Society. (c) A fluorescence

signal amplifier enabled by an enzyme-powered DNA walker migrating on a 2D DNA origami track.[46] Reprinted with permission from 2017 American Chemical Society. (d) An electrochemical sensor for amplified protein detection using a protein-assembled bipedal DNA walker on a DNA-functionalized 2D planner electrode track.[47] Reprinted with permission from 2015 Royal Society of Chemistry.

Peng *et al.* recently described such a system, where a bi-directional 1D DNA walker was used to detect multiple miRNAs through distance-based ECL energy transfer. Specifically, a bipedal DNA walker was designed to be able to walk forward along a 1D DNA track in response to miR-21 and backward in response to miR-155 (Figure 5b).[44] The DNA track was composed of four single strands of DNA (T1, T2, T3, ssDNA) that when mixed, created a double stranded complex with three protruding single strands. These three protruding single strands were partially complementary to the miRNA targets and three attachment strands (A2, A3, B1). The sequential addition of target, addition strands and waste strands (D1) generates forward or backward motion of a walker labeled with a gold nanoparticle (AuNP). To generate a distance-based ECL signal, the DNA track was cast onto the surface of a glassy carbon electrode coated with a film of Mn^{2+} doped CdS nanocrystals (CdS:Mn NCs). The ECL signal would be quenched when the AuNP was in close contact with CdS:Mn NCs and restored when the AuNP was separated from CdS:Mn NCs; both situations were precisely controlled by the target-induced DNA walking. Using this strategy, the detection limits were 1.51 fM for miR-21 in an attenuation assay format and 1.67 fM for miR-155 in a turn-on assay format. In addition to walkers (steppers) that are controlled by adding fuel molecules in each step, it is also possible to harness autonomous 1D DNA walkers for controlling signal transduction. For example, Chen *et*

al. harnessed a classic nicking endonuclease-powered DNA walker design that transduced electrochemiluminescence signals for the detection of DNA targets.[45]

1.5 2D DNA Walkers for Bioanalysis

One limitation of a 1D biosensor is the extent of its processivity; due to the few degrees of freedom of its movement on a DNA track, the number of steps that the DNA walker can take is limited and so is the subsequent level of signal amplification. By introducing a second dimension to the movement, the degrees of freedom are increased and so is the extent of processivity. Therefore, 2D DNA walkers are potentially better signal amplifiers than 1D DNA walkers.[46-50] In 2017, Tinnefeld and coworkers introduced a fluorescence signal amplifier made of a 2D DNA walker (Figure 5c).[46] The 2D track was constructed using DNA origami, where one M13mp18-derived scaffold strand was folded into a rectangle of 100 nm in length and 70 nm in width using 192 staple strands. The single-foot inchworm DNA walker contains a nicking recognition site and the track molecule (stator strand) contains a nicking cleavage site. Driven by nicking endonuclease, the DNA walker traversed the 2D track by consuming the stator strands through nicking cleavage. The processivity was ensured using the toehold-mediated strand displacement reaction. To be used as a fluorescence amplifier, each stator strand was modified with a molecular quencher, which were complementary to the stator strands. Fluorophore-labeled imager DNA sequences were added to the 2D track after DNA walking. While walking, the walker released quenchers through nicking cleavage and thus could turn on the fluorescence of the imager strand, so that the 2D track could be directly visualized under a confocal fluorescence microscope. As each DNA walker was estimated to move for up to 60 steps, linear signal amplification can thus be achieved, increasing the amplification by a unit every step the single-foot walker takes. The fluorescence signal could be further enhanced 15-fold through plasmonic

enhancement, which was achieved by docking a pillar shaped DNA origami between two 80 nm AuNPs.

Besides DNA origami, the 2D track can also be constructed from DNA-functionalized planar surfaces.[47-51] In particular, when an electrode is used as the planar surface, an electrochemical signal can be directly generated and amplified through DNA walking.[47-49] Li *et al.* described the first example of such an electrochemical detection platform that generated amplified detection signals through a DNAzyme-based burnt-bridge bipedal DNA walker (Figure 5d).[47] In particular, the bipedal DNA walker was first split into two parts, each conjugated with an affinity ligand. As such, the complete bipedal DNA could only be assembled through sandwiched affinity binding in the presence of a target protein. The protein-assembled bipedal DNA walker then traveled autonomously on the 2D substrate-modified planar electrode removing the redox label from the electrode surface. By measuring the electrochemical signal attenuation, the authors have quantified as low as 1.5 aM target proteins in buffer and human serum samples. Besides DNAzyme, nicking endonuclease could also be used as the energy input for driving the target-responsive 2D bipedal DNA walker. Ji *et al.* recently developed such a system for the one-step quantification of human α-thrombin on an electrochemical detection platform.[48] In addition to a planar electrode, a glass slide can also be used as a planar surface for constructing the track of a 2D DNA walker. Zhu *et al.* recently described a DNAzyme-driven 2D DNA walker that moved and cleaved quencher-labeled track molecules and thus turned on fluorescence signals in response to a target nucleic acid.[50] Facilitated by fluorescent microscopy and a homemade pixel counting program, the authors could detect as low as 100 fM target nucleic acid using this 2D DNA walker system.

1.6 3D DNA Walkers for Biosensing Applications

Since first introduced by Ellington and coworkers in 2015,[32] the concept and strategies of 3D DNA walkers have made significant impact for developing novel analytical methods for biomolecular analysis. The rapid walking kinetics and high processivity make this class of DNA walker an ideal tool for signal transduction and amplification. Applications range from nucleic acid testing,[51-57] to protein detection,[58-61] cell imaging,[62-64] and probing dynamic interactions on cell membranes.[65]

1.6.1 3D DNA Walker for Nucleic Acid Testing

The first 3D DNA walker was designed to be responsive to nucleic acid targets through the principle of catalytic hairpin assembly (CHA).[32] In this system, the 3D track was constructed by dense functionalziation of a DNA hairpin (H1) on a microparticle through streptavidin-biotin conjugation (Figure 6a). A second hairpin (H2) was also designed, which could potentially hybridize to H1. However, the complementary sequences between H1 and H2 were caged into hairpins and thus the hybridization was kinetically hindered. It is possible to accelerate the reaction between the two hairpins by introducing a catalyst capable of opening H1 through a toehold-mediated strand displacement reaction. By integrating two catalysts into a single DNA sequence, the authors constructed a bipedal DNA walker that could take 36 steps on the 3D track before dissociation. The authors further converted this DNA walker into a biosensor for miR-122 by introducing a "reservoir-particle" that hosted the bipedal walker. Only when the miR-122 was added, was the bipedal walker released into the solution, initiating the CHA reaction and the autonomous DNA walking on the 3D track. By labeling H2 with a fluorescent dye, the authors were able to quantify as low as 1 nM target nucleic acids using flow cytometry. In addition to the bipedal walker design, the same group also demonstrated that it was possible to develop a single-

foot inchworm type of DNA walker by extending the catalyst with a cleat domain, which is a short single-stranded region on the walker that stays processively on the track strands.[51] Compared to the bipedal design, such a cleated DNA walker was more persistent against dissociation and displayed a higher processivity over a longer period of time. The successes of CHA-driven bipedal or cleated DNA walkers proved the possibility of DNA walking on a 3D track system and opened opportunities for novel signal amplification and transduction strategies.[52-55] For example, by integrating a G-quadruplex into CHA, Li *et al.* developed label-free fluorescent assays for amplified detection of the smallpox gene.[52] Other signal read-outs, including chemluminescence,[53] electrochemiluminescence,[54] redox, and color/fluorescent visualization,[55] have been integrated into the CHA-mediated 3D DNA walker systems for the sensitive detection of nucleic acids and proteins.

Despite the high processivity provided by CHA, 3D DNA walkers fueled by hybridization are generally limited by slow kinetics. To address this issue, we have recently introduced a new 3D DNA walking device that was driven by a nicking endonuclease (Figure 6b).[38] The 3D track was fabricated by functionalizing ~400 DNA substrates onto a 20 nm diameter gold nanoparticle (AuNP) through Au-S conjugation. The DNA walker with a 50-nt long polydT spacer was also co-conjugated onto the same AuNP. The substrate DNA, containing a nicking cleavage site, was labeled with a fluorescent dye that was initially quenched by the AuNP. The DNA walker contained a nicking recognition site and thus could cleave the substrates. In the presence of the nicking endonuclease, release of the cleaved sequence from the AuNP is detected by the fluorescence of the (now unquenched) fluorophore in solution. As all DNA motifs were localized on each 20 nm AuNP, this 3D DNA walker demonstrated remarkably high processivity and fast mass transfer. The cleavage of all substrates required ~20 min. To further convert this 3D DNA

walker into a biosensor for a target nucleic acid, we deactivated the DNA walking by introducing a protecting strand that hybridized with the walker and partially blocked the nicking recognition site. A toehold domain was also designed on the protecting DNA, so that it could be efficiently removed by the target nucleic acid sequence through a toehold-mediated strand displacement and thus restored the activity of the 3D DNA walker. By measuring the initial rate of walking as the readout, we were able to quantify as low as 5 pM tuberculosis-specific DNA within 20 minutes. Using an endpoint reading at 60 min, we managed to further push the detection limit to 300 fM.

The endonuclease-driven 3D DNA walker is also compatible with other nucleic acid detection platforms. For example, Zhang *e. al.* developed an ultrasensitive electrochemiluminescence biosensor for Kras mutations which integrated the 3D DNA walker with hyperbranched RCA.[55] Xu *et al.* demonstrated the combined uses of the endonuclease-powered 3D DNA walker with exonuclease-mediated signal amplification for quantifying miR-141 on an electrochemical detection platform.[57] In addition to nicking endonuclease, exonuclease III has also been used to construct the stochastic 3D DNA walker on AuNP.[39] In particular, Qu *et al.* demonstrated that the rationally designed 3'-end protected DNA walker acted as an inchworm DNA walker traversing the 3D DNA-AuNP track (Figure 6d).[39] By tuning the track density on the AuNP, the authors were able to control the dynamic range of the 3D DNA walker for quantifying the target nucleic acid sequence. Remarkably, when a low density DNA track was used, the detection limit was pushed to 10 fM.

1.6.2 3D DNA Walker for Protein Detection

To convert the 3D DNA walker into protein-responsive biosensors, it is critical to integrate affinity binding motifs into the DNA walker and the 3D track to facilitate the target recognition

and signal transduction. Zhang *et al.* demonstrated a universal binding-induced assembly strategy that expanded the nicking endonuclease-powered 3D DNA walker to proteins (Figure 6c).[58] In this system, the 3D track consisted of a 20 nm AuNP that was co-conjugated with hundreds of fluorescently labeled track molecules and several anchor strands labeled with an affinity ligand. A DNA walker containing the nicking recognition site was also labeled with another affinity ligand that bound to the same protein target but at a different binding affinity. In the presence of the target, the sandwiched binding between the two affinity ligands to the same protein assembled the DNA walker on the 3D track, which cleaved hundreds of track molecules and amplified fluorescence signals. Using this system, the authors were able to achieve a high processivity of over 100 steps and detected as low as 0.5 pM streptavidin and 5 pM platelet-derived growth factor BB (PDGF-BB), respectively. Having developed the protein-responsive 3D DNA walker, the same group also demonstrated that it is also possible to drive this system using DNAzymes by replacing nicking cleavage substrates with DNAzyme-specific substrates.[59] In both works, fluorescently labeled track molecules were used for direct signal generation. It is also possible to translate the protein binding event into the release of DNA barcode molecules for subsequent reactions or signal amplification. We have previously developed a binding-induced molecular translator, making use of binding-induced DNA strand displacement.[60] However, this molecular translator was limited by the fact that one target protein could maximally release one DNA barcode. Using the idea of the 3D DNA walking, we were able to address the current challenge and create a binding-induced molecular amplifier capable of translating a single input protein into the release of hundreds of pre-designed barcode DNA in a single-step.[61]

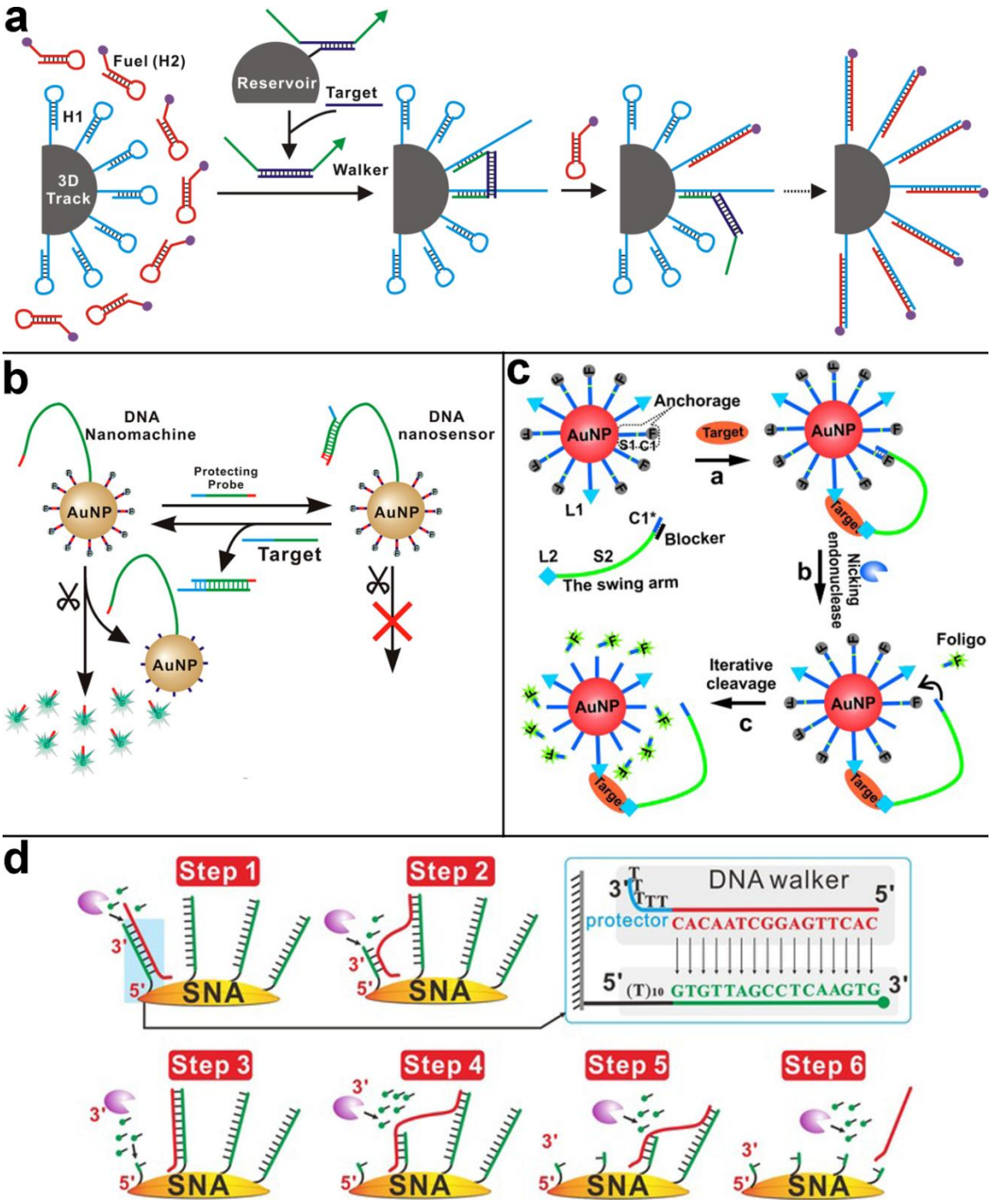

Figure 6. Schematic illustration of biosensors making use of DNA walkers traversing on 3D tracks. (a) Detection of microRNA using microparticle-based stochastic 3D DNA walker powered by catalytic hairpin assembly.[32] (b) Nicking endonuclease-driven 3D DNA nanomachine for amplified detection nucleic acids.[38] Reprinted with permission from 2016

American Chemical Society. (c) Binding-induced molecular motor that translates affinity binding into on-particle DNA walking and subsequent signal amplification.[58] Copyright 2015 John Wiley and Sons. (d) A stochastic on-particle DNA walker driven by exonuclease III for sensitive detection of nucleic acid targets.[39] Copyright 2017 John Wiley and Sons.

1.6.3 3D DNA Walker for Cellular Analysis and Imaging

AuNPs, densely functionalized with DNA molecules used to provide 3D track for DNA walkers can be readily and efficiently taken up by cells without the need for transfection agents.[62] Such a unique advantage promotes the application of the 3D DNA walker to cellular analysis and imaging. In 2017, Le and coworkers constructed one of the first 3D DNA walker systems that could be operated in living cells. This system was created by co-conjugating both DNA walker and track molecules onto 20 nm AuNPs (Figure 7a).[63] The DNA walker contained a truncated form of 8-17E DNAzyme and the track molecules were the substrates for this DNAzyme. Initially, the DNA walker was deactivated by a complementary locking sequence. Once delivered into the cell and in the presence of the target microRNA (miR-10b), the DNA walker was activated by removing the locking sequence through a toehold-mediated strand displacement reaction. To track the 3D DNA walker intracellularly, the locking sequence was labeled with a Cy5 dye. The operation of the 3D DNA walker was triggered by adding Mn^{2+} as the co-factor and monitored by labeling the track molecules with fluorescin amidite (FAM). By doing so, the authors were able to quantify 1pM of miR-10b within an aggressive form of breast cancer cells (MDA-MB-231) in an operation time of 60 min, under physiological pH and Mn^{2+} concentration. Another 3D DNA walker capable of imaging intracellular microRNA was recently described by Liang *et al.*, where entropy-driven DNA catalysis was adopted to power the DNA walking on the 3D DNA-AuNP track.[64,65]

In addition to imaging intracellular nucleic acid targets, 3D DNA walkers also found unique applications to probing the dynamic and transient molecular encounters on live cell membranes. Unlike other 3D DNA walkers where spherical nano- or microparticles were used as tracks, the cell surface walkers developed by You *et al.* were inserted into the cell membrane through lipophilic labels and harnessed the whole cell membrane as the track for the DNA walking (Figure 7b).[66] The on-membrane migration of the walker (anchor site) was driven by diffusion and the subsequent strand displacement rate was linearly correlated with the rate of encounters between anchor sites. This unique 3D DNA walker system was capable of measuring the encounter dynamics of two anchor sites or two target membrane components. Using this 3D DNA walking device, the authors have successfully monitored the rapid encounter events of membrane lipid domains using flow cytometry and fluorescence microscopy and revealed a preference for encounters within the same lipid domains.

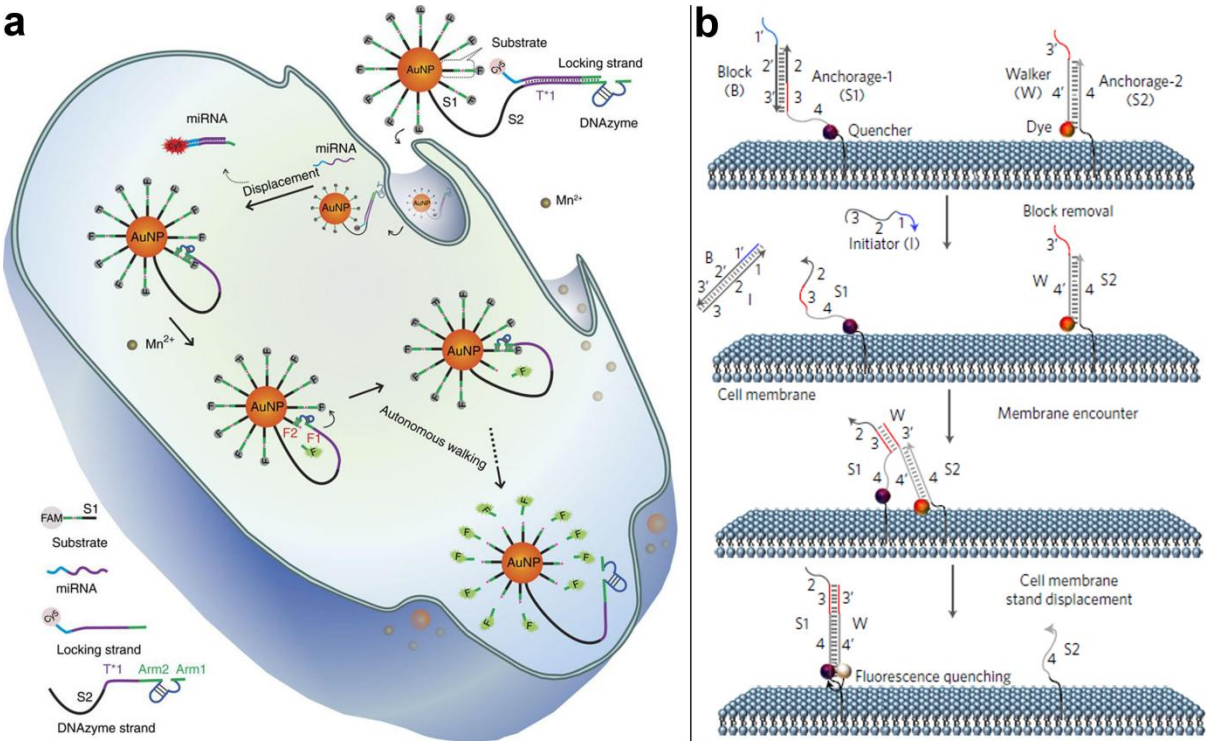

Figure 7. (a) Amplified detection and imaging of intracellular microRNA using a 3D DNA walking device driven by DNAzyme.[63] Reprinted with permission from 2017 Springer Nature. (b) Probing dynamic and transient molecular encounters on live cell membranes using DNA walker that diffuses on cell membrane as the track.[66] Copyright obtained from 2017 Springer Nature.

1.7 Conclusions and Perspective

The development of novel DNA machines and devices for bioanalytical applications has been a focus of analytical nanoscience and nanotechnology over the past two decades. Analytical tools fabricated using the concept and strategies of DNA walkers have only appeared in the last several years but are rapidly increasing in both quantity and quality. The recent realization of 2D and 3D DNA tracks has unleashed the signal amplification power of DNA walking devices, which is essential for quantifying and imaging minute amount of biomolecules in test tubes or

living cells. Because of their high processivity and directionality, DNA walkers have also played critical roles in designing signal transduction pathways for homogenous and surface-based biosensors. To maximize the signal amplification capacity, DNA walkers driven by enzymatic cleavage or non-covalent DNA catalysis are the most popular choices for analytical tool development. Other types of walking mechanisms, such as cell membrane bound DNA walkers driven by diffusion,[65] have demonstrated unique advantages and applications. Another unique advantage of DNA walkers is the potential to overcome the mass transfer barrier, which is a critical concern for many surface-based biosensors in terms of shortening the sample-to-answer time. So far, this unique potential has been largely limited by the slow kinetics of procession of many DNA walkers. However, Walter and coworkers have recently created a cartwheeling DNA walker driven by toehold-exchange with a stepping rate constant approaching 1 s^{-1}, which is 10- to 100-fold faster than prior DNA walkers.[67] This exciting finding suggests that the slow kinetics of procession of most DNA walkers is a fundamental limitation, rather the result of insufficiently optimized designs. Similarly, a recent study of localized DNA hybridization chain reactions on DNA origami have revealed that the localized on-surface signal transduction can be independent from the diffusion of DNA strands for each step and thus can provide faster reaction kinetics.[68] Given rapid growth for designing and optimizing better DNA walkers and great attentions received from the analytical community, we anticipate that the unique properties of this class of dynamic DNA nanotechnology will be continuously explored and sharpened for fabricating superior analytical tools with wide applications to disease diagnosis, bioimaging, and deciphering biological processes in the near future.

1.8 Objective and Hypothesis

In this thesis work, we aim to advance the new and promising direction of using DNA walkers and 3D DNA tracks for analytical applications such as biosensor development. Although the above works have shown rapid growth for designing and optimizing better DNA walkers, including the use of substrate functionalized AuNPs to generate 3D tracks, the biophysical process by which a DNA sequence "walks" at the biomolecule-nanoparticle (bio-nano) interface, such as the surface of 3D DNA (SNA) tracks, remains unexplored. Therefore, we hypothesize that better understanding of varying interfacial factors such as valence, binding hindrance, adsorption, orientation and curvature effects that occur at the bio-nano interface between the DNA walker, the DNA track and the inorganic AuNP surface will enable better design and operation of DNA walker for diverse analytical applications. The study will also lead to new insights of biorecognition and enzymatic behaviours at bio-nano interfaces in general. Therefore, we propose to develop a series of DNA walkers that traverse on 3D SNA tracks and probe various interfacial factors using these constructs (Chapter 2). We also apply the knowledge gained from this study to guiding the design of novel biosensors for amplified detection of nucleic acids, proteins, and small molecular targets (Chapter 3). Chapters 2 and 3 were modified from our recent publication in ACS nano.[69]

Chapter 2

Probing and Controlling Dynamic Interactions at Biomolecular –Nanoparticle Interfaces Using Stochastic DNA Walkers

2.1 Introduction

Biohybrid inorganic nanoparticles (NPs) have offered exciting opportunities in material science with applications ranging from biosensing[70-73], to gene regulation[74], to drug delivery, and to the fabrication of novel structures and devices[75-77]. While much effort has been emphasized on the synthesis, functionality, and applications of novel NPs, it is also critical to understand and control dynamic interactions at the biomolecular-nanoparticle (bio-nano) interfaces. This is because molecular interactions, such as affinity binding and enzymatic catalysis at bio-nano interfaces, are often influenced by multiple interfacial factors, such as valence, binding hindrance, adsorption, orientation[78,79], and curvature effects[80,81], and thus may differ significantly from those in bulk solutions. It has been well documented that multivalent, ligand-modified NPs are often of enhanced binding affinities compared to isolated ligands. A growing number of recent studies also suggest that polyvalent, substrate-modified NPs can accelerate enzymatic reactions compared to freely diffused substrate in bulk solution[82,83]. On the other hand, Seferos *et al.* found that DNA substrates functionalized to gold NPs (AuNPs) presented a strong resistance to degradation by deoxyribonuclease I[84]. In a following study, Pridogich *et al.* further demonstrated that it was possible to regulate enzyme activities using the DNA-AuNP interface which selectively enhanced ribonuclease H while inhibiting other nucleases[85]. Given the unique role of bio-nano interfaces in mediating molecular interactions, strategies capable of fine-tuning and probing the interfacial environment might lead to new insights and thus open new opportunities for guiding the better design and uses of NPs.

This chapter outlines the development of biohybrid nanoparticles and their uses in material sciences, including acceleration, inhibition and regulation of enzymatic activities using substrate loaded onto the surface of NPs, and the limitations of understanding interfacial interactions at this bio- nano interface. This chapter will show our objective, to develop stochastic DNA walkers to probe the bio- nano interface and understand all potential interfacial interactions. This chapter has been modified from from our recent publication in the journal ACS Nano.[69]

2.2 Objectives

Herein, we report an approach to rationally design and assemble a series of enzymatic systems with tunable interfacial microenvironments and thus allow the interrogation of the specific roles of varying factors at the bio-nano interface. The idea of using DNA walkers to probe the bio-nano interface is inspired by the recent advances of stochastic DNA walkers capable of traversing on three dimensional (3D) tracks made of spherical nucleic acids (SNA)[6,38,39,58,89]. We hypothesize that enzyme-powered stochastic 3D DNA walkers are an ideal system to probe and control dynamic interactions at bio-nano interfaces. Contrary to existing enzyme-NP systems, where intraparticle movement of enzymes are dominated by nonspecific adsorptions, the persistent movement of DNA walkers and subsequent enzymatic reactions are mediated by Watson-Crick base-pairing and thus are highly predictable and programmable. As such, we design a SNA track and a series of DNA walkers and demonstrate the unique roles of varying interfacial factors, including adsorption, orientation, co-operativity, steric effect, multivalence, and binding hindrance.

2.3 Results and Discussion

2.3.1 Design Principle of DNA Walkers

Molecular interactions at the bio-nano interface may differ significantly from that of a bulk solution. For example, enzymatic activities in a bulk solution are dominated by molecular colliding (Scheme 1A), the kinetics of which can be quantitatively described using the classic Michaelis-Menten (MM) model (eq. 1)

$$V = V_{max}\frac{[S]}{K_M+[S]} \qquad (1)$$

$$V_{max} = k_{cat}[E]_0 \qquad (2)$$

where V is the rate at a substrate concentration [S], K_M is the Michaelis constant, V_{max} is the maximum rate which is determined by the catalytic rate constant k_{cat} and initial enzyme concentration $[E]_0$ (eq. 2). However, enzymatic activities can be far more complicated at the bio-nano interface, involving intraparticle interactions resulting from non-specific adsorption and varying interfacial factors (Scheme 1B).[74-79] An ideal substrate-NP system for probing enzymatic activities shall allow the independent control and interrogation of each factor. As such, we designed a series of nicking endonuclease powered stochastic 3D DNA walkers with the SNA track as the bio (DNA)-nano (AuNP) interface. Each walking step involves the following three elementary reactions:

Reaction 1: $S + W \underset{k_{-1}}{\overset{k_1}{\rightleftharpoons}} SW$

Reaction2: $SW + E \underset{k_{-2}}{\overset{k_2}{\rightleftharpoons}} SWE$

Reaction 3: $SWE \xrightarrow{k_{cat}} W + E + P$

where *W* represents the DNA walker, *S* represents the substrate, *E* is the nicking endonuclease and P is the product, cleaved substrate from the SNA. When supplying excess amount of nicking endonuclease, intermediates *SW* and *SWE* will be consumed rapidly. The quasi-steady-state assumption can thus be applied, where

$$\frac{d[SW]}{dt} = k_1[S][W] + k_{-2}[SWE] - k_{-1}[SW] - k_2[SW][E] = 0 \quad (3)$$

$$\frac{d[SWE]}{dt} = k_2[SW][E] - k_{-2}[SWE] - k_{cat}[SWE] = 0 \quad (4)$$

The rate of the overall reaction *V* can then be derived as:

$$V = \frac{d[P]}{dt} = \frac{\frac{k_1 k_2 [E] k_{cat} [W]_0}{k_1 k_2 [E] + k_1 k_{-2} + k_1 k_{cat}} \cdot [S]}{\frac{k_{-1} k_{-2} + k_{-1} k_{cat} + k_2 [E] k_{cat}}{k_1 k_2 [E] + k_1 k_{-2} + k_1 k_{cat}} + [S]} \quad (5)$$

As nicking endonuclease is in large excess, [E] can be replaced with $[E]_0$ and the equation can be further simplified as:

$$V = \frac{{V_m}^* \cdot [S]}{{K_m}^* + [S]} \qquad (6)$$

where:

$${V_m}^* = \frac{k_1 k_2 [E]_0 k_{cat} [W]_0}{k_1 k_2 [E]_0 + k_1 k_{-2} + k_1 k_{cat}} = k^*_{cat} [W]_0 \quad (7)$$

$${K_m}^* = \frac{k_{-1} k_{-2} + k_{-1} k_{cat} + k_2 [E]_0 k_{cat}}{k_1 k_2 [E]_0 + k_1 k_{-2} + k_1 k_{cat}} \quad (8)$$

The mathematical derivation of eq. (6) suggests that the behavior of a DNA walker (*W*) follows the MM model, as eq. (6) is the same as eq. (1) and eq. (7) is the same as eq. (2), given $[E]_0$=

$[W]_0$ since nicking endonuclease is in large excess, and therefore, BDW is effectively an enzyme in our system.

The design of a specific bipedal DNA walker (BDW) is illustrated in Scheme 1C. The SNA track is created by conjugating hundreds of fluorescently labeled single-stranded DNA (ssDNA) substrate to a 20 nm AuNP through the well-established gold-thiol chemistry.[87,88] Each substrate contains a 7-nt nicking cleavage sequence. BDW is a ssDNA containing the 7-nt nicking recognition sequence (the foot) at both 5' and 3' ends. Because of the base complementarity, BDW can bind to the SNA track at the DNA-AuNP interface. In the presence of nicking endonuclease, BDW cleaves the substrate and walks along the interface (intraparticle interaction). When both feet cleave substrates at the same time, BDW dissociates and diffuses back into the bulk solution. As each walking step releases a fluorophore labeled cleavage product, the dynamic interactions between BDW and track can be monitored in real-time. Varying interfacial factors can be controlled and probed by introducing variants in the walker or tuning the SNA track.

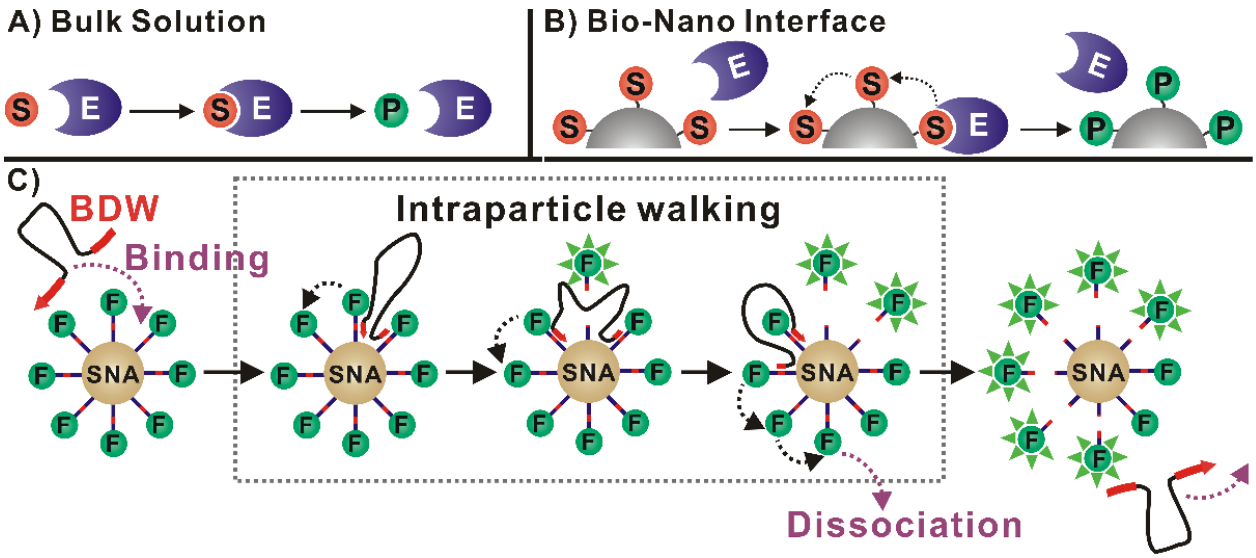

Scheme 1. Schematic illustration of enzyme-substrate interaction in bulk solution (A) and at the bio-nano interface (B). (C) An enzyme-powered bipedal DNA walker (BDW) capable of traversing at the bio-nano interface created by a spherical nucleic acid (SNA) track. The red domains of BDW represent nicking recognition sequences and those of SNA substrates represent nicking cleavage sequences. The nicking endonuclease is omitted from the figure for better presentation.

2.3.2 Intraparticle Interactions

Intraparticle interactions between enzyme and a substrate are one of the most important interfacial factors that complicate the enzymatic behavior at the bio-nano interface. Depending on the reversibility of the intraparticle interaction, an enzymatic reaction at the bio-nano interface can be modeled as a hopping mechanism or a scooting mechanism. In a hopping mechanism (Figure 8A), an enzyme adsorbs onto the surface of the nanoparticle and hydrolyzes substrate, followed by a dissociation back into the solution where it can adsorb again onto the same nanoparticle, or a different nanoparticle to hydrolyze substrate molecules, thus making the

interaction reversible. In a scooting mechanism (Figure 8C), an enzyme will adsorb onto the surface of the gold irreversibly, and therefore may only hydrolyze substrate on that nanoparticle.[79] However, in most of the enzymatic systems, intraparticle interactions are driven by nonspecific adsorption which is difficult to control and measure. Therefore, the exact role of intraparticle interaction and the enzymatic behavior at the bio-nano interface can only be deduced through indirect measurements and mathematical fitting[73]. Towards this challenge, we first set out to engineer two DNA walker systems that provide programmable intraparticle interactions through DNA hybridization.

The BDW was designed to have two 8-nt feet at both 3' and 5' ends (Table 1). As a result, BDW can bind stably with the SNA track in the absence of the nicking endonuclease. To quantitatively probe the role of intraparticle interaction, we designed two SNA tracks that were of the same substrate sequence and density (~150 per SNA) but labeled with fluorescent amidite (FAM, F-Track) and tetramethyl rhodamine (TAMRA, T-Track), respectively (Figure 8A). BDW was first pre-hybridized on the F-Track and then mixed with the T-Track and then nicking endonuclease. By monitoring fluorescence signals produced by both tracks in real-time (Figure 8B), we found that BDW reacted predominately on the F-track during the first 6 min with an average rate of 2 substrates cleaved per NP per minute. The signal from the T-track then increased drastically beginning at 7 min. Correspondingly, a near 4-fold drop of the cleavage rate was also observed at the F-Track. This suggests that each BDW cleaves FAM-labeled substrates on the F-Track SNA to which it is originally bound before completely dissociating and subsequently binding to a T-Track SNA in solution. Therefore, the reversible intraparticle interaction has led to a hopping mechanism and each BDW could take, on average, 12 persistent steps at the SNA interface before hopping to another NP. To assemble an enzyme-NP system with irreversible intraparticle

interaction, we next modified the BDW by replacing the 5’ nicking recognition sequence with a 12-nt poly-A foot that hybridizes to the poly-T spacer of the substrate (Figure 8C). Therefore, the tethered DNA walker (referred as TDW) (Table 1) can be irreversibly hybridized on the SNA track through the 5' poly-A foot while the 3’ foot remains enzymatically active. Once primed on the F-track and interrogated using the T-Track (Figure 8C), we found that TDW cleaved predominately on the T-Track (Figure 8D). This is evidenced by the rapid cleavage of F-Track substrates until all were cleaved near the 30 minute mark, resulting in a saturation of the signal (green), coupled with very little cleavage of substrate on T-Track, resulting in very little signal increase (red), suggesting that a scooting mechanism could be realized through an irreversible intraparticle interaction.

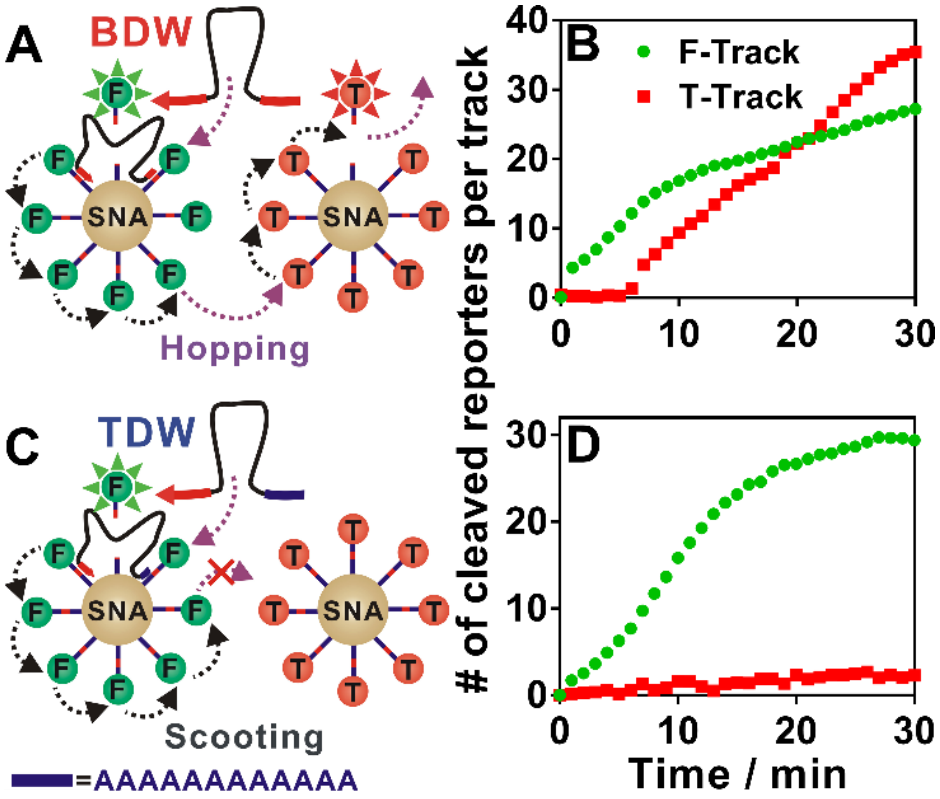

Figure 8. Probing and controlling intraparticle interactions using bipedal DNA walkers. (A) Probing reversible intraparticle interactions commonly involved in enzymatic reactions at the bio-nano interface using a BDW and two fluorescently labeled SNA tracks: F-Track, which contains FAM fluorophore on the substrate, and T-Track, which contains TAMRA fluorophore on the substrate. (B) Kinetic profile of BDW that is initially primed on F-Track and then mixed with T-Track. [BDW] = 250 pM, [F-Track] = [T-Track] = 500 pM, [nicking endonuclease] = 1 unit. (C) Probing the role of irreversible intraparticle interactions on the kinetics of enzymatic reactions at the bio-nano interface using a tethered DNA walker (TDW). (D) Kinetic profile of TDW that is initially primed on F-Track. [TDW] = 250 pM, [F-Track] = [T-Track] = 500 pM, [nicking endonuclease] = 1 unit

We also pre-hybridized BDW to T-Track and added F-Track to the solution to observe a hopping mechanism (Figure 9). Although we observed no substrate cleavage on the F-Track SNA for the

first several minutes, we did not observe a drastic increase in F-Track substrate cleavage at any point, nor a subsequent decrease in the rate of substrate cleavage on the T-Track, like we did when BDW was primed to the F-Track, which suggests BDW consistently prefers T-Track over F-Track under the same substrate sequence and density, suggesting that subtle chemical changes (TAMRA over FAM) at the bio-nano interface may also significantly alter the enzymatic behavior.

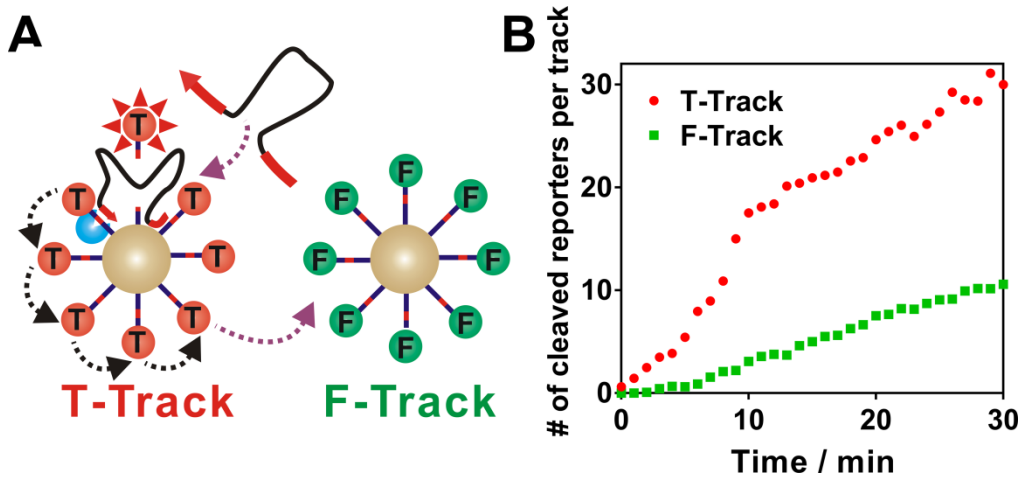

Figure 9: Probing the activity of BDW by priming it onto the T-Track first and then exposing it to F-Track and nicking endonuclease. (**B**) Real-time monitoring the kinetic performance of BDW on T-Track (red) and F-Track (green), respectively. [T-Track] = [F-Track] = 500 pM, [BDW] = 250 pM, and the density of both tracks were ~150 substrates per SNA.

2.3.3 Orientation, Co-operativity, and Steric Hindrance

When densely functionalized on a NP, DNA substrates may behave significantly different from those in a homogenous solution. Such heterogeneity also complicates the biorecognition and enzymatic activities at bio-nano interfaces. The steric hindrance and nearest-neighbor interactions often hinder mutually favorable orientations between enzyme and substrate[75]. The multivalence, on the other hand, may promote enzymatic activities through enhanced binding

affinity and cooperativity[77-79]. To probe and control each interfacial factor, we engineered the BDW into a series of DNA walkers to have enhanced impact on orientation, co-operativity, or steric hindrance (Figure 10).

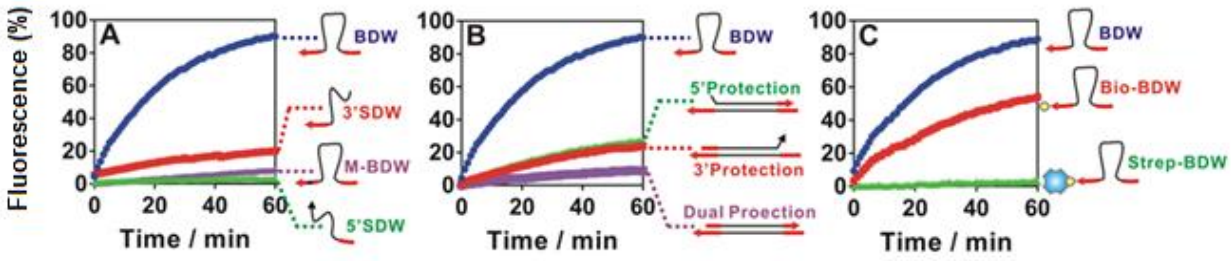

Figure 10. Quantitatively determining the effect of orientation (A), co-operativity (B) and steric hindrance (C) on enzymatic activities at the bio-nano interface using varying DNA walker designs. In all experiments, [Walker] = 500 pM, [F-Track] = 500 pM, [nicking endonuclease] = 1 unit. The concentration of streptavidin is 1 nM. The fluorescence signals were normalized by using a positive control containing 500 pM BDW and the SNA track (the saturated signal was set to be 100) and a negative control containing only the track

We first probed the effect of orientation by modifying BDW into two single-foot DNA walkers that only contain the 3'-foot (3'SDW) or the 5'-foot (5'SDW) (Sequences in Table 1). When compared to the BDW, 3'SDW and 5'SDW became much less efficient at cleaving substrate from the SNA (Figure 10A). This is confirmed by BDW reaching near 100% saturation in 60 minutes, but 3'SDW reaches only ~25% and 5'SDW reaches ~5%. This is to be expected, as there is no second foot to facilitate intraparticle walking. More importantly, though the sequences are identical for both single feet, the 3'SDW maintained a near 25% activity while 5'SDW maintained 5% activity, suggesting that the orientation of the walker played a critical role at the interface. More specifically, to maintain the anti-parallel base-pairing with substrates,

the 5’SDW needs to fold its orientation to expose the nicking recognition sequence, whereas the 3’SDW can insert readily into the substrate layer (Figure 11). Despite the disfavored orientation, we also found that the 5’ foot of BDW may still bind and cleave the substrate, evidenced by the observation that BDW with a deactivated 3’-foot (M-BDW) (Table 1) could still maintain nearly 10% activity (Figure 10A). The 3' foot on M-BDW is deactivated by a single base mutation within the nicking recognition sequence of the 3' foot. This mutation allows for the foot to still bind to the substrate at the seven complementary bases, but the mismatched DNA within the nicking recognition site prevents the nicking endonuclease from binding to the 7nt duplex, and hydrolyzing the substrate strand.

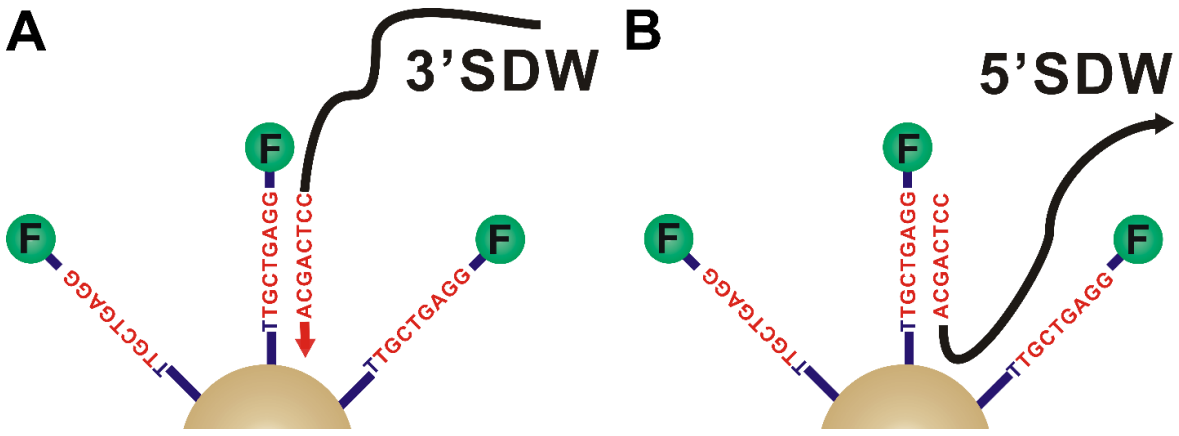

Figure 11: Comparing Orientation of 3'SDW and 5'SDW with the substrate on SNA. (A) Polarity required for anti-parallel base-pairing between 3'SDW and substrate allows for direct insertion onto the SNA. (B) Polarity required for anti-parallel base-pairing between 5'SDW and substrate requires the walker to fold over in order to bind to the substrate on the SNA. Despite the disfavoured orientation, 5'SDW may still bind and cleave substrate at an efficiency of roughly 10%.

To further understand the role of orientation for the BDW, we selectively deactivated the 3' foot or 5' foot by introducing a protecting DNA that partially blocks the nicking recognition sequences through hybridization (Figure 10B) (Protecting DNA sequences in Table 1). We have previously shown that this strategy could completely deactivate a DNA walker that was co-conjugated with substrates on the same AuNP.[82] When placing the protection at the 5'-foot, the BDW was effectively deactivated, with an activity (~30% of the unprotected walker) slightly higher than that of the 3'SDW (~25%). Surprisingly, when placing the protection at 3' end, the activity of BDW was still 30%, which was significantly higher than that of the 5'SDW. This observation is consistent with our speculation that the 5' foot could still initiate binding with a SNA (Figure 10A), which brings the protected 3' foot in close proximity to the substrate. As a result, the activity of 3' foot could be partially restored through a strand displacement between substrate and the protecting strand. A near complete deactivation could only be achieved when both feet were deactivated through hybridization (Figure 10B: dual protection), suggesting that a strong co-operativity exist between the two feet upon binding to the SNA track. We also found that the co-operativity between the two feet of the BDW were distance and rigidity dependent. An optimal spacer length of 18 nt was found to maximize the kinetics of cleavage (Figure 12). All the BDW with varying spacer length (L1, L6, L12, L18, L24) are found in Table 1.

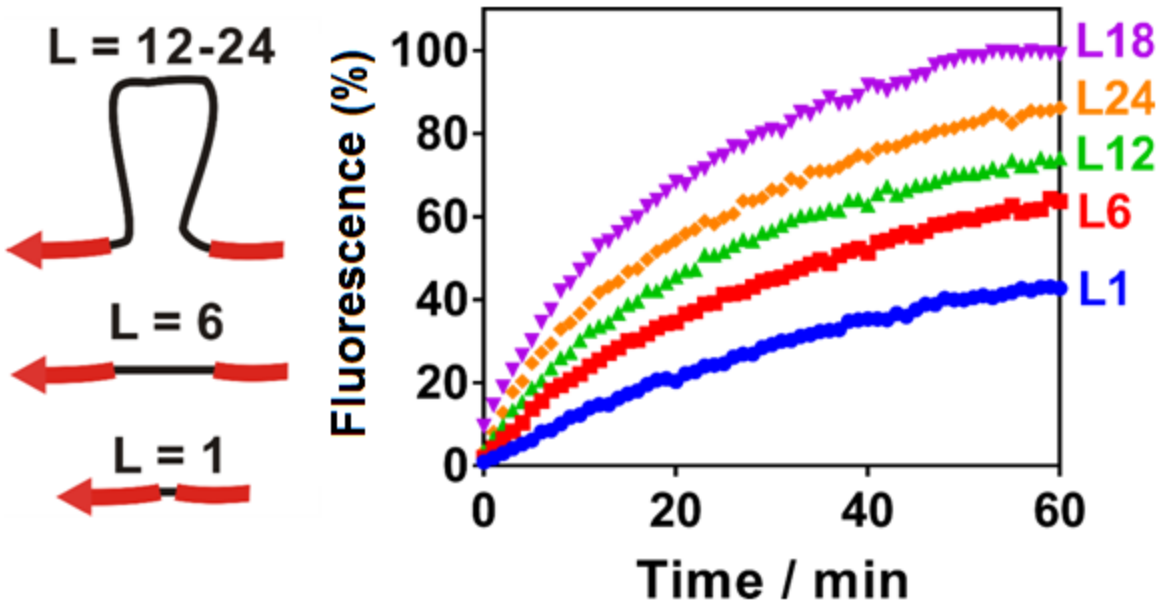

Figure 12: Effect of the spacer length on the kinetic performance of BDW. The length of the spacer spans from L = 1 nt to L = 24 nt. [F-Track] = 500 pM, [BDW] = 1 nM.

By replacing the flexible 15nt ssDNA spacer of the BDW with a more rigid duplex spacer, we observed a reduction of activity by approximately 30%. (Figure 13).

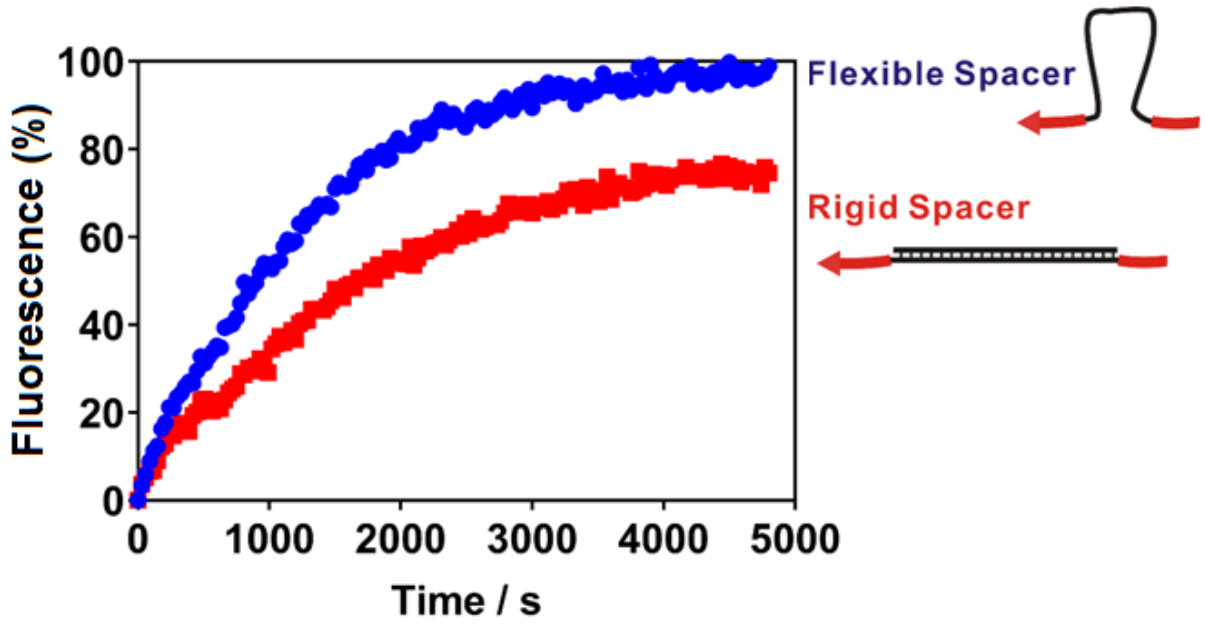

Figure 13: BDW with a 15nt ssDNA linker vs. BDW with a more rigid 15nt dsDNA linker. By making the linker region more rigid by introducing a complementary strand of DNA, the activity of BDW was decreased by around 30%.

We finally probed steric effects by chemically modifying the BDW with a biotin molecule at the 3' end (Figure 10C). This chemical modification slightly increases the bulkiness of the BDW, which resulted in a decrease of activity by ~30% (Figure 10C: Bio-BDW). The activity of the BDW was almost completely deactivated when a large bulky streptavidin was bound to biotin at the 3' end through the strong streptavidin-biotin interaction (Figure 10C: Strep-BDW), suggesting the steric hindrance may become significant when bulky groups exist at the bio-nano interface, such as a biotin-streptavidin conjugate, which would have a size of roughly 5-6nm[89,90].

By probing the effect of each interfacial factor, we were able to better understand the enzymatic behavior at the bio-nano interface. The proposed mechanisms for the four representative DNA walkers are outlined in Scheme 2. The BDW is the most efficient DNA walker because of the favored orientation at 3' end, the high binding co-operativity, and intraparticle interactions (Scheme 2A). Although there was only one foot, the 3'SDW maintains a ~25% activity because of the favored orientation (Scheme 2B). For a 5'SDW, the 5' foot may still bind to the SNA track, but because of the disfavored orientation and binding hindrance, it can dissociate rapidly before triggering enzymatic cleavage (Scheme 2C). The streptavidin-biotin-modified BDW, on the other hand, completely blocks the 3' foot of BDW from binding to substrate and enzymatic reactions, leading to a near complete deactivation of BDW (Scheme 2D).

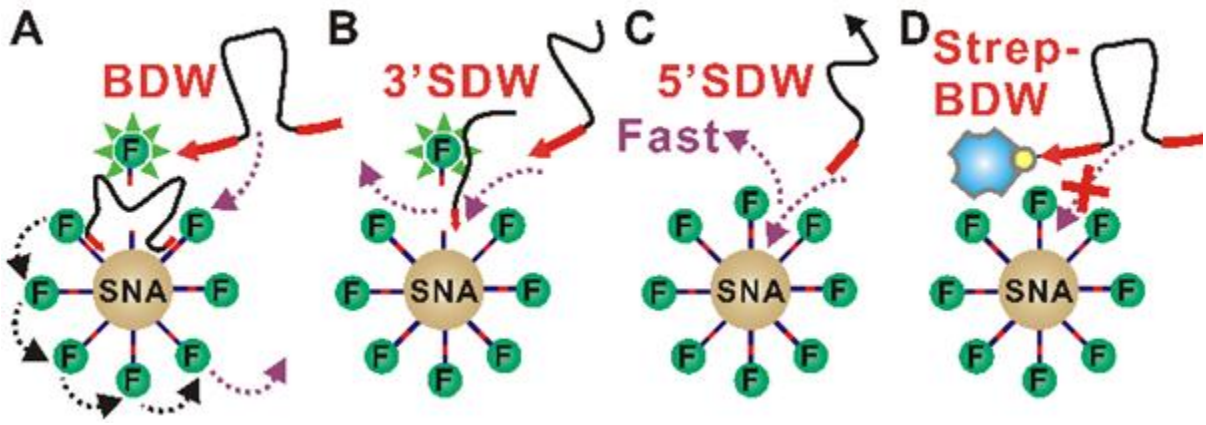

Scheme 2. Proposed mechanisms of (A) BDW, (B) 3'SDW, (C)5'SDW, and (D) streptavidin-modified BDW for binding and interacting with SNA track.

2.3.4 Multivalence *vs.* Binding Hindrance

Having investigated varying interfacial factors by designing a series of DNA walkers, we then explored the impact of the interfacial environment on intraparticle interactions and the initial binding between the BDW and SNA track. The interfacial environment, such as the density of

substrate on each SNA, has a direct impact on important interfacial factors such as multivalence, which is the amount of substrate per NP and binding hindrance (steric hindrance and charge repulsion) between the negatively charged DNA backbone on the substrates and BDW, as well as the negatively charged surface of the AuNP. Therefore, we aim to control the interfacial environment by fine-tuning the substrate density at the SNA interface.

We first explored the impact of [BDW] on intraparticle interaction. We found that V is linearly related to the concentration of BDW (Figure 14A-C), suggesting that the apparent catalytic rate constant k_{cat}* is also independent of the interfacial environment. The initial rate was estimated using data points collected in the first 5 min. The concentrations of BDW were lower than those of the F-track in all cases. Next, we explored the impact of substrate density on the intraparticle interaction. To exclude the influence of the initial binding step, the BDW was primed on the SNA before subjecting the hybridized BDW-substrate to enzymatic cleavage. By monitoring the initial intraparticle walking in real-time, we found that the initial rate V of the enzymatic reaction was independent from the density (Figure 14D-F). $[S]_{total}$ was determined as a product of F-track concentration and average numbers of substrate on each track. In this set of experiments, the track concentration was kept at 500 pM with densities varying from 150 per track to 400 per track and [BDW] was kept at 500 pM. The intraparticle walking was found to be a zero-order reaction with respect to $[S]_{total}$ (F), suggesting that intraparticle walking is independent of the substrate concentration in the bulk solution. This observation is consistent with our speculation that the local effective concentration of substrate on each track is much higher than K_m*, therefore V equals to V_{max} and thus independent of the substrate concentrations.

We found that the initial rate V of the enzymatic reaction was independent from the concentration of SNA (Figure 14G-I). [BDW] was kept at 100 pM and the density of the track

was ~150 substrates per track. The intraparticle walking was also found to be a zero-order reaction with respect to the concentration of F-tracks (I), confirming that each SNA track was an isolated system during the initial intraparticle walking stage. This result suggests that the intraparticle interaction was dominated by the local effective concentrations of substrates rather than the multivalence or binding hindrance. The effective concentration ([S]) remains much higher than K_M* (eq. 6) because of the ultra-small volume the reactants occupying (< 30 zL) and high effective concentration (> 200 μM). Therefore, V equals to the maximal initial rate V_{max} throughout varying experimental conditions (eq. 7).

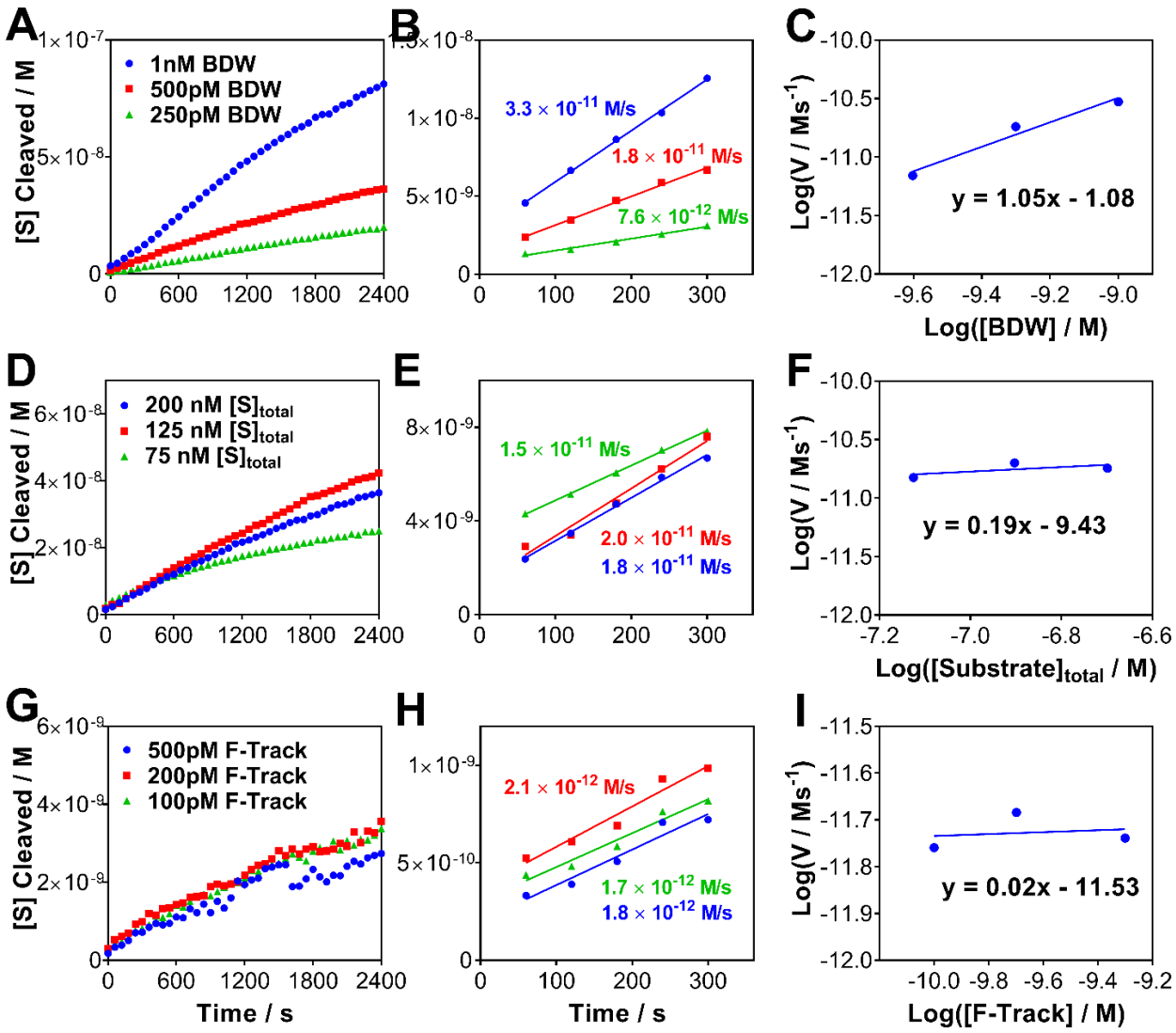

Figure 14. Determining kinetic order of intraparticle walking.

The concentration effect can be described quantitatively using the MM kinetics (eq. 6):

$$V = \frac{V_m^* \cdot [S]}{K_m^* + [S]} \qquad (6)$$

$$V_m^* = \frac{k_1 k_2 [E]_0 k_{cat} [W]_0}{k_1 k_2 [E]_0 + k_1 k_{-2} + k_1 k_{cat}} = k_{cat}^* [W]_0 \quad (7)$$

$$K_m{}^* = \frac{k_{-1}k_{-2} + k_{-1}k_{cat} + k_2[E]_0 k_{cat}}{k_1 k_2 [E]_0 + k_1 k_{-2} + k_1 k_{cat}} \quad (8)$$

where the effective concentration ([S]) is always much higher than K_M because of the ultra-small volume the reactants occupying (< 30 zL) and high effective concentration (> 200 μM). Therefore, V equals to the maximal initial rate V_{max} throughout our experimental conditions (eq. 7). We also found that V is linearly related to the concentration of BDW, suggesting that the catalytic rate constant k^*_{cat} is also independent of the interfacial environment.

We next evaluated the effect of substrate density on the binding between the BDW and the SNA, as both multivalence and binding hindrance may have a direct but opposite impact on the binding step. However, it is difficult to directly probe the binding step by monitoring the fluorescence, as it is coupled with the subsequent intraparticle walking. As such, we introduced a low-density T-Track as a reference interface, which was mixed with either a high-density F-Track (HD-Track, ~400 substrates per SNA) (Figure 15A) or a low-density F-Track (LD-Track, ~150 substrates per SNA) (Figure 15B). Upon mixing with BDW, the two tracks (T-Track and F-Track) compete for binding with BDW. We then measured the initial rates of cleavage on both tracks using the fluorescence signals in both channels, and took the ratio ($V_{F\text{-}Track}/V_{T\text{-}Track}$), which was plotted in Figure 15C. The ratio for the HD- F-Track was found to be 4-fold higher than that of the LD- F-Track, suggesting that multivalence dominates the binding step and interface of higher substrate density is more competitive for binding.

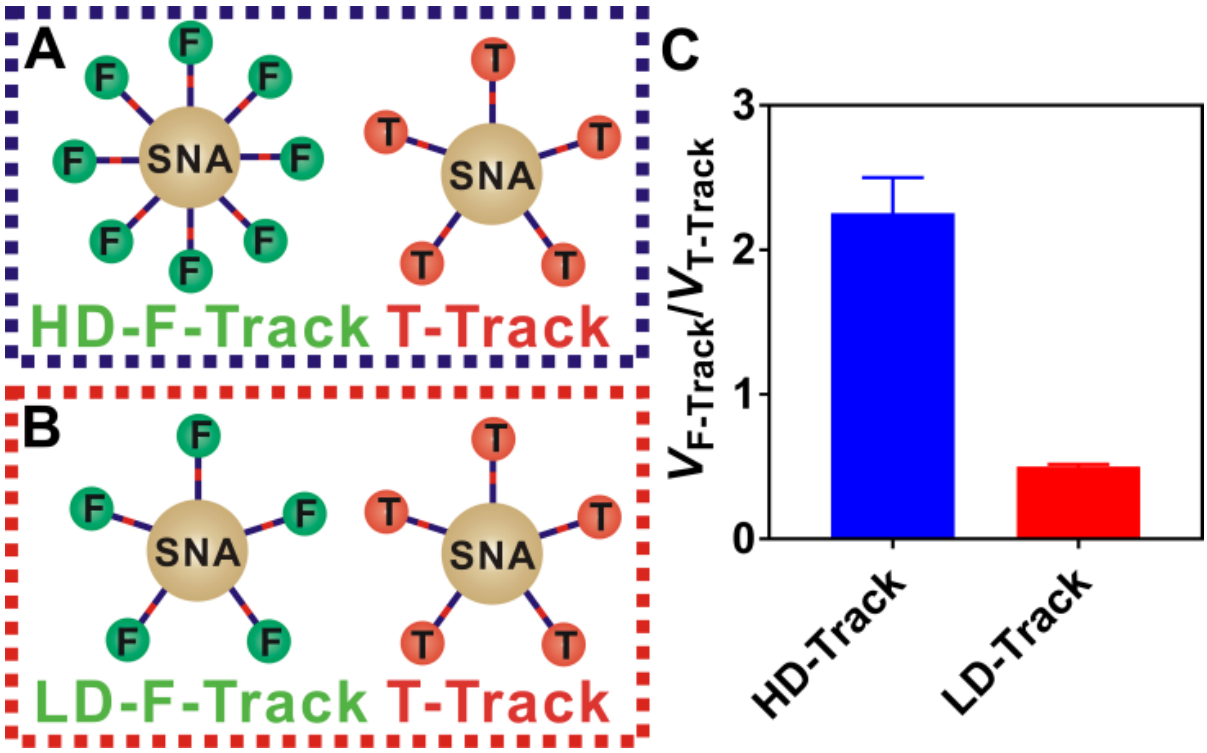

Figure 15. Effect of interfacial environment (multivalence *vs.* binding hindrance) on the initial binding between BDW and SNA track. BDW is interrogated using a mixture of high-density (A) (HD) F-Track and a reference low-density (LD) T-Track or a mixture of (B) low-density (LD) F-Track and a reference LD T-Track. (C) Comparing the ratio of initial rates between F-Track and reference T-Track for HD-Track and LD-Track, respectively. [BDW] = 250 pM, [HD-F-Track] = [LD-F-Track] = [T-Track] = 500 pM, [nicking endonuclease] = 1 unit. Each error bar represents one standard deviation from triplicate analyses.

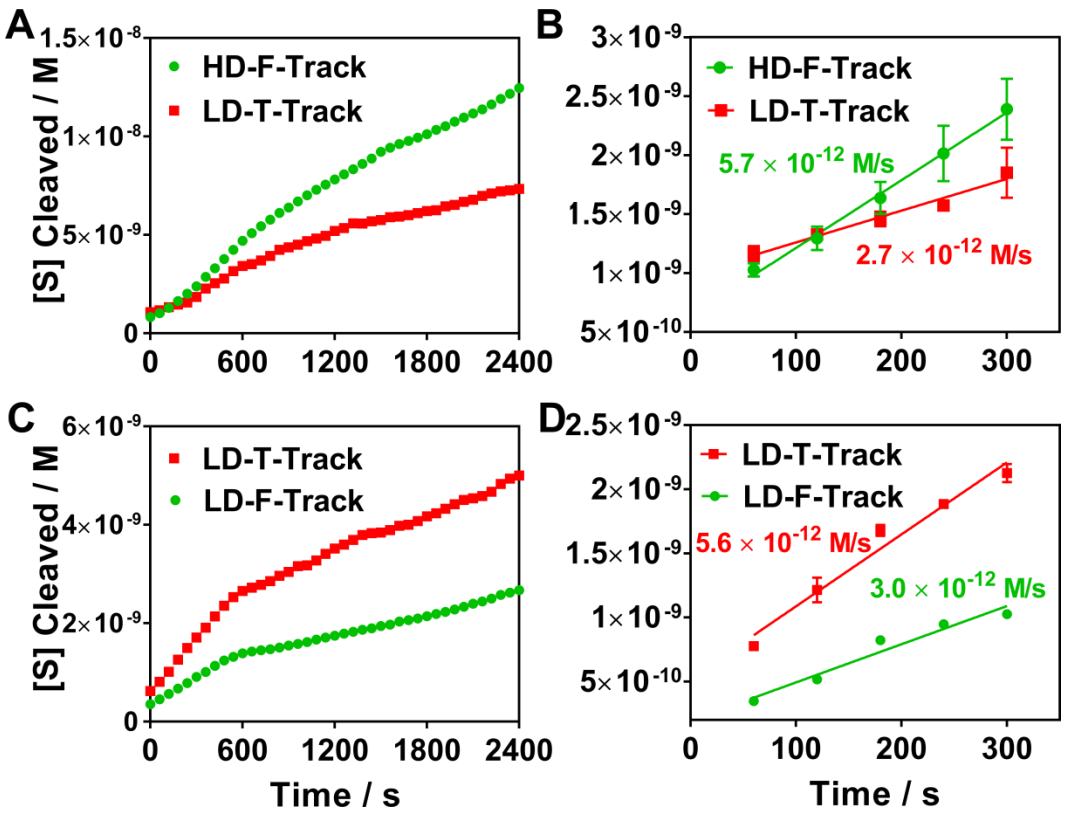

Figure 16. Effect of substrate density on the initial binding between BDW and SNA track. (A) Real-time monitoring fluorescence increases in both high density (HD) F-track and low density (LD) T-track when adding BDW to a mixture of equal concentrations of both tracks. (B) The initial rates for both tracks were determined using data points in first 300 s. (C) Real-time monitoring fluorescence increases in both high density LD-F-track and LD-T-track when adding BDW to a mixture of equal concentrations of both tracks. (D) The initial rates for both tracks were determined using data points in first 300 s. [HD-F-Track] = [LD-F-Track] = [LD-T-Track] = 500 pM, [BDW] = 250 pM. The densities for both LD-F-Track and LD-T-Track were estimated to be ~150 substrates per SNA track. The density for HD-F-Track was ~400 substrates per SNA track.

Finally, given that the 3' foot and 5' foot have different binding affinity to substrate, and when DNA is densely functionalized onto the surface of a NP, the activity of 5'SDW is only ~5% compared to BDW, we set out to explore if decreasing the density of the F-Track results in a more active 5'SDW or 5' foot of BDW. This was done by comparing an activity ratio between the 5'SDW and 3'SDW at different density of F-Track (Figure 17). Figure 17A shows the activity of 3'SDW and 5'SDW on a high density (~400 substrates/ F-Track) F-Track (HD-F-Track), Figure 17B shows the activity of 3'SDW and 5'SDW on a medium density (~250 substrates/ F-Track) F-Track (MD-F-Track) and Figure 17C shows the activity of 3'SDW and 5'SDW on a low density (~150 substrates/ F-Track) F-Track (LD-F-Track). Figure 17D compares the activity ratios (5'SDW/ 3'SDW). Our findings were consistent with earlier observations that binding hindrance is more significant for the 5'SDW that is sensitive to the binding orientation. As the F-Track density decreased, we see an increase in activity ratio (Figure 17D).

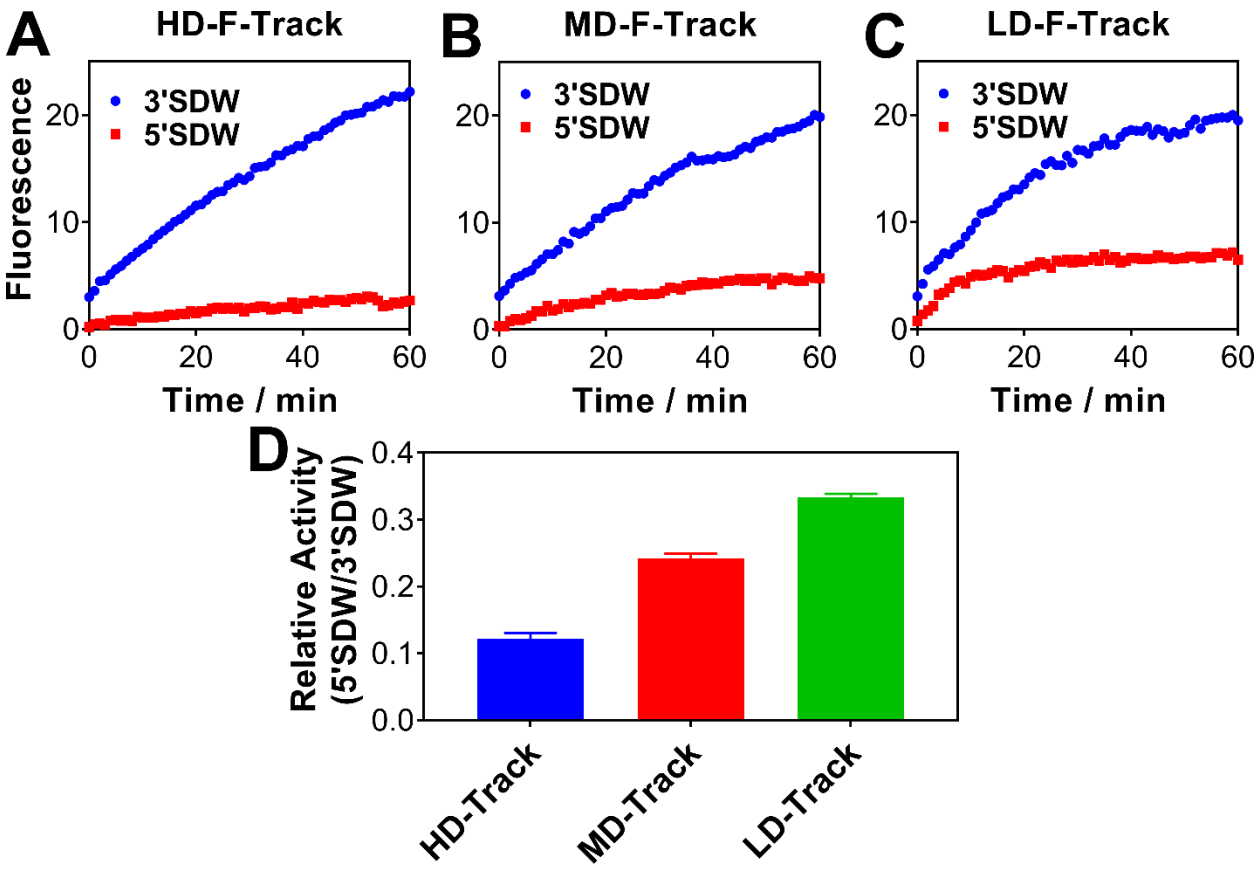

Figure 17. Effect of substrate density on the performance of 5'SDW. Activities of 5'SDW on (A) high-density track (HD-Track, ~400 substrates per SNA track, (B) medium-density track (MD-Track, ~250 substrates per SNA track, and (C) low-density track (LD-Track, ~150 substrates per SNA track, were monitored in real-time. As 3'SDW is insensitive to the steric hindrance of the interface, it was used here as a reference. (D)The fluorescence signal ratios between 5'SDW and 3'SDW at 60 min were plotted for comparison. [HD-Track] = [MD-Track] = [LD-Track] = 100 pM, [5'SDW] = [3'SDW] = 1 nM.

2.3.5 Conclusions

We have developed an approach to assemble a series of stochastic DNA walkers capable of probing and controlling dynamic interactions at bio-nano interfaces. By monitoring dynamics of these DNA walkers on SNA tracks, we have systematically investigated the effect of important

interfacial factors on enzymatic activities at the bio-nano interface. These include intraparticle interaction, orientation, co-operativity, steric effect, multivalence, and binding hindrance, Our mechanistic study has revealed critical roles of bio-nano interfaces for enzyme activities and the performance of nanosensors and nanodevices. Several factors can be used based on our findings to create and optimize a biosensor using BDW. First, DNA walkers with multiple binding and catalytic sites may drastically improve its activity through cooperative binding and intraparticle interactions. Second, the strong co-operativity of a bipedal DNA walker may require a protection strategy that deactivates both active sites. Third, the density of a SNA track shall be maximized to enhance the binding. Fourth, DNA walkers are sensitive to both orientation and steric hindrance. A biosensor may be designed by selectivity manipulate these properties in a target-specific manner.

Chapter 3

Design and Application of DNA-Walker based Biosensors for the Detection of Nucleic Acids, Proteins and Small Molecules

3.1 Introduction

Our objective is to develop nucleic acid, protein and small molecule biosensors using a DNA walker and substrate-loaded AuNP as a signal readout method based on the knowledge gained probing the bio-nano interface using BDW (Chapter 2). This chapter has been modified from from our recent publication in the journal ACS Nano.[69]

3.2 Designing DNA Walkers for Biomolecule Detection

Using the newly gained knowledge of the bio-nano interface, we introduce three novel biosensors for amplified detection of nucleic acids, proteins and small molecules. Our mechanistic study exploring dynamic interactions at the bio-nano interface (Chapter 2) revealed several critical factors that can be used for better design of biosensors involving interfacial interactions. For example, the conversion of our DNA walker system into biosensors can be rationalized by considering the following criteria drawn from the mechanistic study in the previous chapter. First, DNA walkers with multiple binding sites (feet) may improve the activity, meaning fluorescent signal release, through cooperative binding and intraparticle interactions. Second, the strong co-operativity of a bipedal DNA walker may require a protection strategy that deactivates both active sites (Figure 10B) in order to suppress fluorescent signal release. Third, the density of a SNA track should be maximized to enhance the binding. Fourth, bipedal DNA walkers are sensitive to both orientation and steric hindrance of binding site at the SNA. A novel biosensor may be designed by selectivity manipulating these properties using a target molecule. To fulfill the potential for translating our newly gained knowledge for biosensor

development, we show three specific approaches for designing nucleic acid, protein and small molecule sensors, respectively.

3.3 Results and Discussion

3.3.1 Rational Design of a Nucleic Acid Biosensor

We first develop a nucleic acid sensor by sequestering a BDW using a protection sequence and then releasing the BDW in a target-specific manner. As suggested in our mechanistic study, we maximized the density of SNA track to achieve favored binding. BDW contains a 15nt linker throughout the nucleic acid sensor design. We also designed a protection sequence (Chapter 2, Section 3.3) that blocked both 3'- and 5'- feet to achieve a complete deactivation of the BDW. However, this protection probe contains two sequence domains (4* and 6*) (Figure 18) that are pre-defined by the nicking endonuclease. As such, the target sequence must be decoupled from the sequence of the protection probe (*i.e.* the sequence of the BDW). As such, we introduced an entropy-driven catalytic DNA circuit that selectively releases the BDW in response to an input target (T).[91] As illustrated in Figure 18, the BDW is fully deactivated in a triplex substrate (S) containing a long ssDNA that is complementary to the BDW at domains 4*, 5* and 6*. S also contains a complementary sequence to T at domains 1* and 2*, but with domains 2* and 3* protected by W1. Target (T) reacts with S through the toehold domain (1*) which releases W1 and exposes another toehold (3*) on S. A fuel (F) strand then initiates a second strand displacement reaction with S through domain 3* and releases BDW, T and a waste duplex W2. BDW can then bind to the SNA track to produce the fluorescence signal. T triggers another cycle of strand displacement. As a result, each target can release multiple BDW-substrate complexes for subsequent enzymatic reactions.

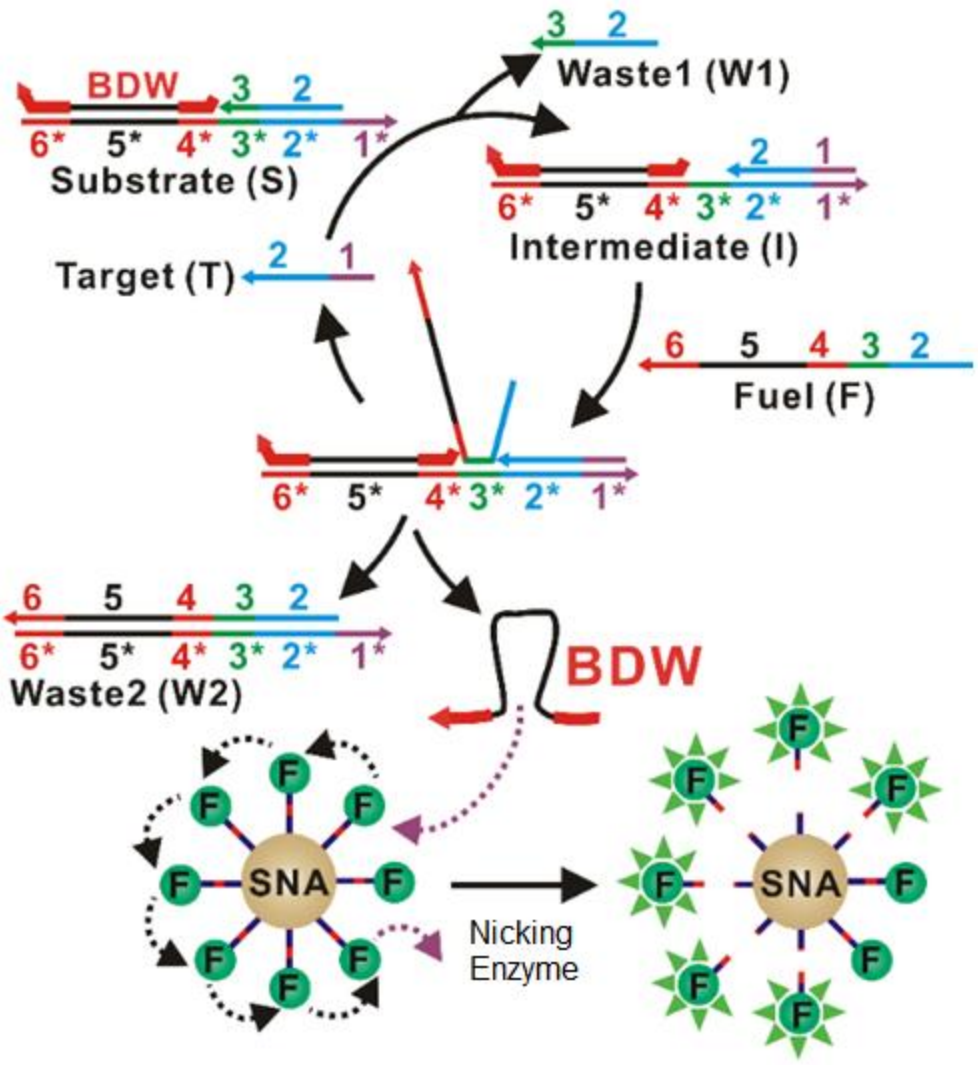

Figure 18. Schematic illustration of target-specific activation of BDW using an entropy-driven catalytic DNA circuit.

3.2 Optimization of the Entropy-Driven Catalytic DNA Circuit

3.3.2 Effect of W1 concentration on BDW deactivation

The first optimization parameter studied was determining the BDW/S/W1 ratio required to fully deactivate the BDW. As illustrated in Figure 10B, single foot protection of BDW results in suppression of fluorescence signal by ~70%. Therefore, the S strand protects both feet of BDW,

but S contains two sequence domains that are pre-defined by the nicking endonuclease, meaning the target sequence must be decoupled from the sequence of protection probe (*i.e.* the sequence of BDW, 6* & 4*) (Figure 18). Sufficient S and W1 are required for full deactivation of BDW, but if very high concentrations are required, excess S and W1 will consume free F and T in solution without contributing to the catalytic circuit. Figure 19 outlines the result of varying the triplex concentration on the fluorescence signal as a function of time. We found that a 1:2:4 BDW/S/W concentration ratio fully deactivated the BDW, as there was no BDW released to create a fluorescence signal. A 1:1:1 ratio still revealed a signal activity of ~ 20% of that positive control, which consisted of free BDW and F-Track.

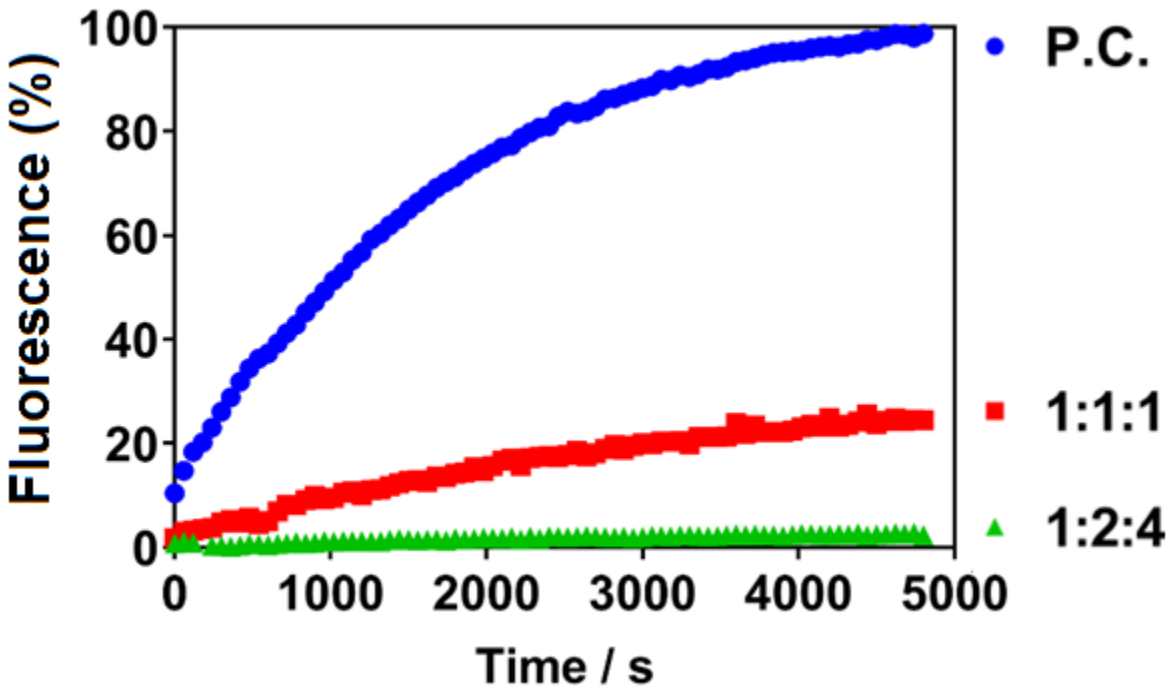

Figure 19. Evaluation of background of varying BDW/S/W triplex concentration ratios (1:1:1 *vs.* 1:2:4). [F-Track] = 500 pM, for 1:1:1, [BDW]:[S]:[W]= 2 nM. For 1:2:4, [BDW]= 2nM, [S]= 4nM, [W]= 8nM.

3.3.3 Effect of Concentration of Fuel Strand on BDW Activity

The next parameter explored was whether or not the F strand affected the activity of the BDW. In the catalytic circuit, the F strand plays the role of releasing the target strand and BDW from S, once the target strand has displaced W1 and a toehold on the 3* region is revealed on S. When BDW and W1 are hybridized to S, there is no free toehold available to react with the F strand (Figure 18), so no activity of BDW should be observed. However, in Figure 20, we found that F generated BDW activity in the absence of target in solution to open the 3* toehold. As the concentration of F increased, the amount of BDW released also increased. Equimolar concentration of 10nM F and S resulted in the release of roughly 50% of deactivated BDW. Therefore, it is necessary to truncate the F strand to avoid unwanted strand displacement reactions.

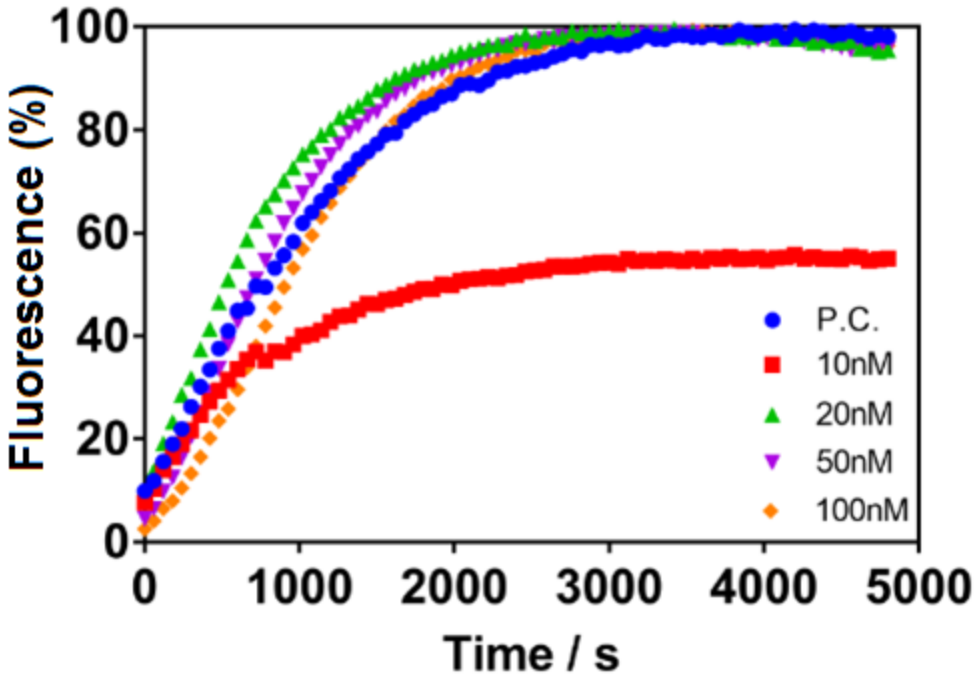

Figure 20. Effect of increasing F concentration on release of protected BDW in solution in the absence of target. (5nM BDW, 10nM S, 12.5nM W1).

3.3.4 Optimization of F length

After finding that F induces strand displacement of BDW and W from the S strand in the absence of target, we explored whether truncating the original length of F resulted in a decrease BDW activation (Figure 21). By shortening region 6 on the 3' end of F, to create F2, we found that the activation of BDW decreased. By removing region 6 from F (F3), the signal was further reduced, closer to that of the negative control (no fuel).

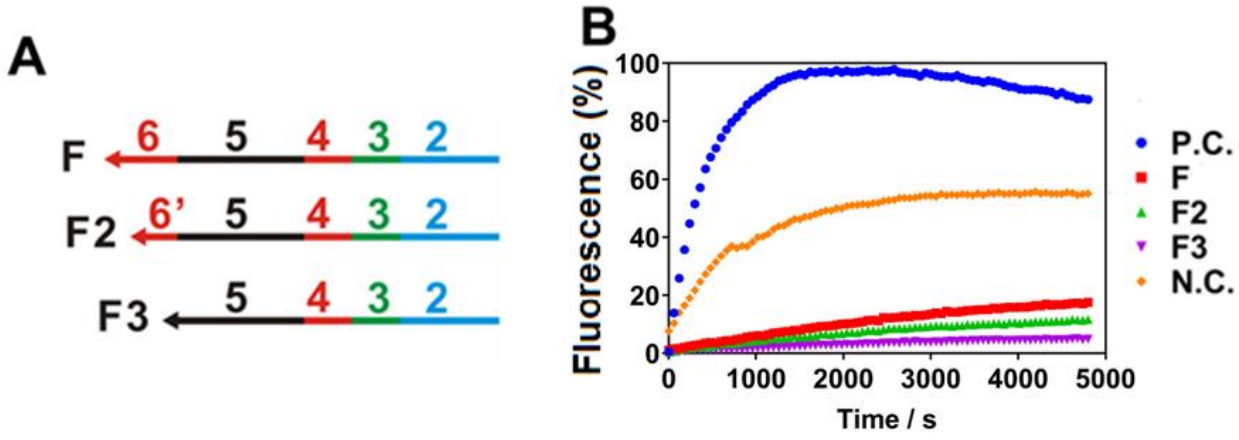

Figure 21. Optimization of the catalytic DNA circuit for nucleic acid sensing. (**A**) Design of the fuel (F). F2 and F3 are truncated versions of F. Sequences are listed in Table S1. (**B**) Evaluation of fluorescence of DNA circuits using varying fuel strand designs (5nM BDW, 10nM S, 12.5nM W1, 10nM F = F2 = F3). P.C. is the positive control which is the BDW and F-Track, N.C. is the negative control which is BDW/S/W triplex and no F strand.

3.3.5 Determining Optimum [W1] for BDW Deactivation

Figure 22 shows the results for changing the concentration of W1 on the deactivation efficiency of the S/W1 blockers on the BDW, given the preliminary observation from Figure 19 that W1 does play a role in BDW deactivation. The [BDW] and [S] were kept constant and [W1] was increased. The result shows that there is no advantage to using a specific concentration of W1, as long as [W1] is $\geq$ 2x [BDW], shown in Figure 22.

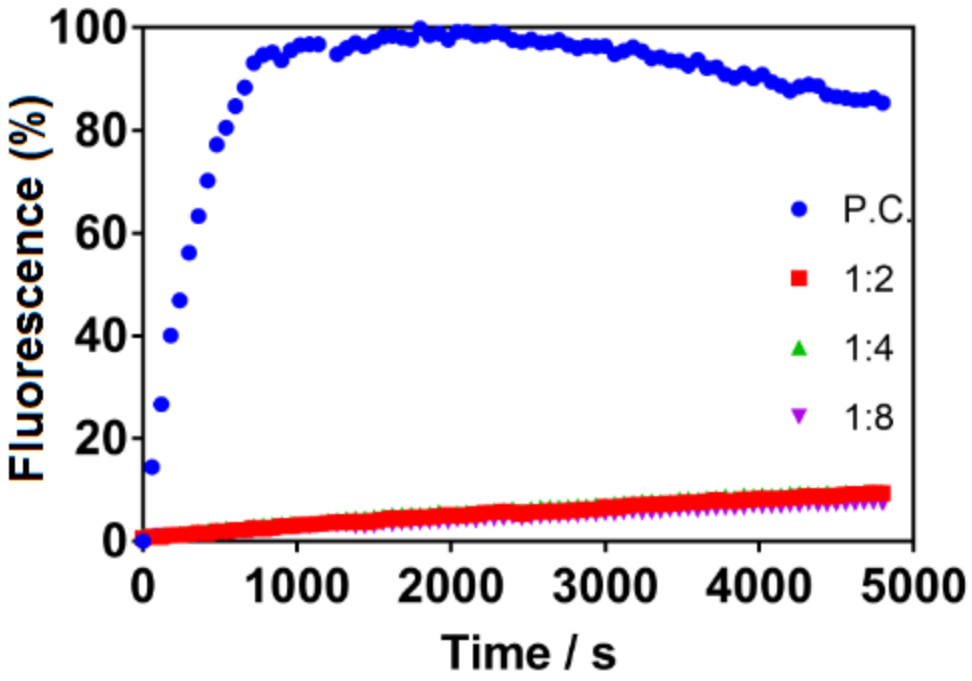

Figure 22. Comparing increased [W1] on complete deactivation of BDW (5nM BDW, 10nM S). Ratios indicate [BDW]:[W1], therefore Red = 10nM W1, Green = 20nM W1, Purple = 40nM W1. Green and purple data points (for W1 = 20nM and 40nM) fall underneath the red (W1= 10nM) data points, indicating there is no advantage to using a specific W1 concentration, so long as [W1] ≥ 2x [BDW].

3.3.6 Optimization of [F3] for BDW Release

We then quantified the optimum [F3] to add to the system. Since F1 and F2 both generated higher background signals in the absence of target (Figure 21B), F3 was used in subsequent experiments given the lower background signal generated. Therefore, we aimed to determine how much F3 could be added to the system without increasing the background signal because the more fuel in the CDC, the greater the rate of BDW and T release, which would result in the greatest signal amplification. The results are shown in Figure 23. There was very little difference

in background signal when [F3] was varied from16nM to 60nM, meaning that we can use a high [F3] to try to generate more signal amplification.

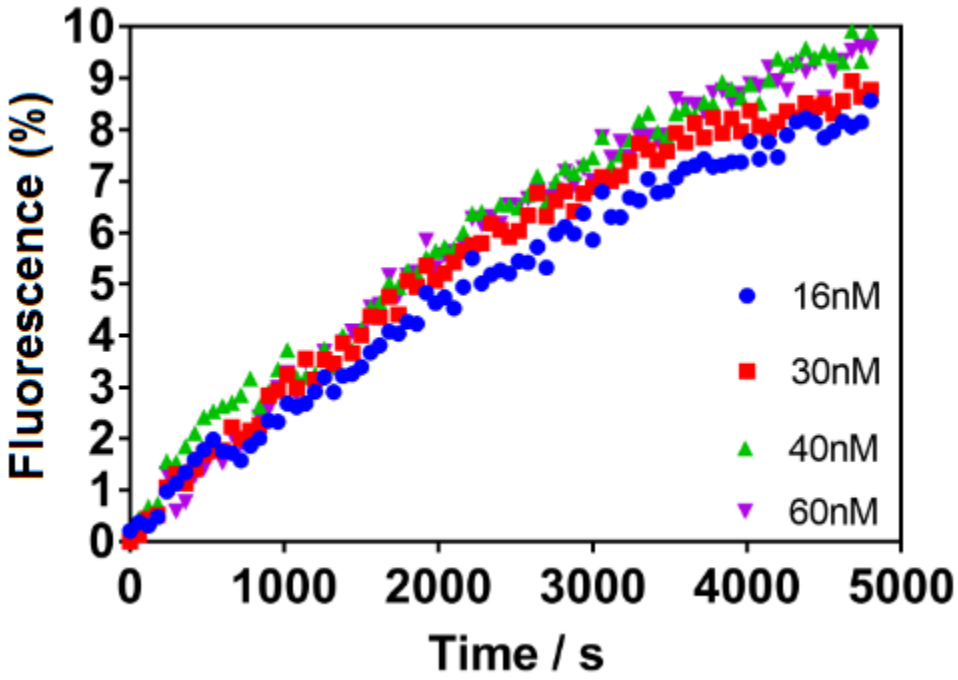

Figure 23. Effect of increasing the [F3] on the release of protected BDW in solution in the absence of target (2nM BDW, 4nM S, 8nM W1). (100% Fluorescence generated by the BDW positive control).

3.3.7 Optimization of CDC Incubation

Finally, we studied varying duration of incubation of the BDW/S/W1 triplex with T and F3 to determine the incubation time required to generate the highest signal-to-noise ratio. We expect that as the incubation time is increased, the signal-to-noise ratio will also increase. Rationally, this is because the longer the incubation, the greater the amplification and thus the more BDW released that will bind to the SNA upon its addition to the incubated solution. Figure 24 shows the result. Based on the error bars shown, the difference in incubation time between 30 min to

180 min is not significantly different. However, for the subsequent experiments for nucleic acid detection using the CDC, we used a 180 min incubation.

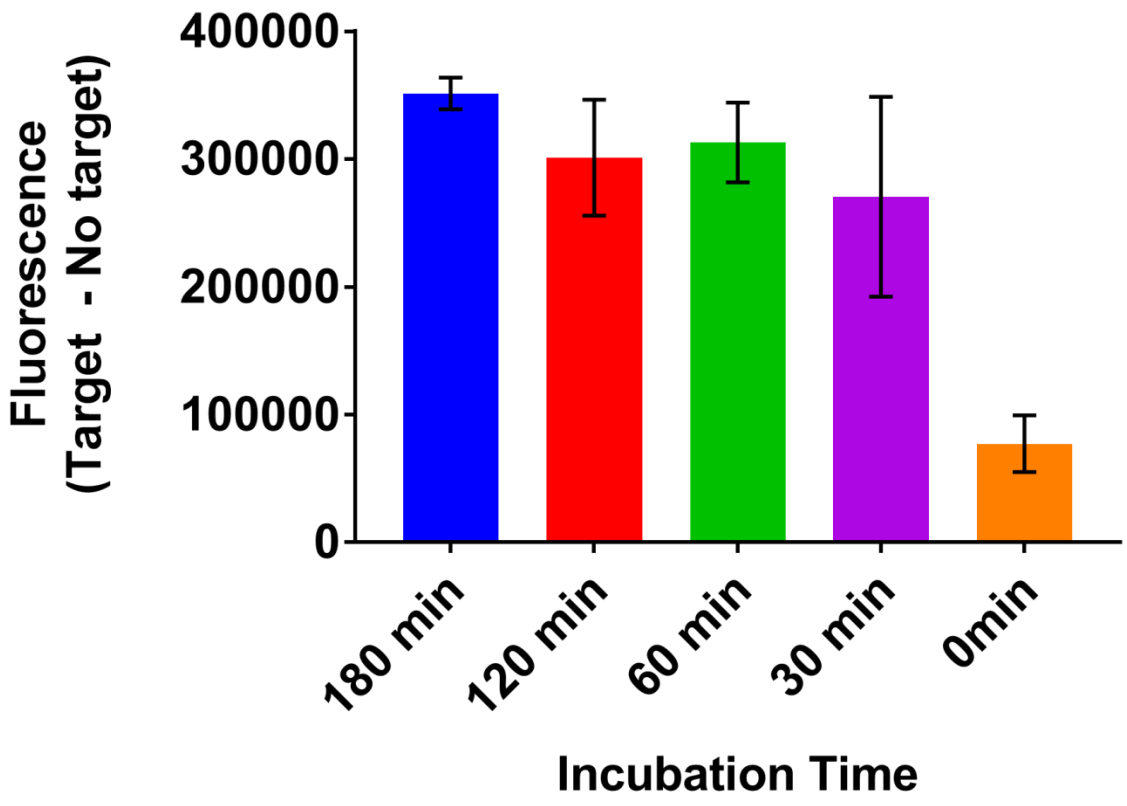

Figure 24. Comparing the difference in fluorescence signal of CDC released BDW on F-track in the presence and absence of 10pM target concentrations at different incubation times. The longer the incubation time (180 min) was not significantly different from any incubation times longer than 0 min (2nM BDW, 4nM S, 8nM W1, 40nM F3).

3.4 Dynamic Range and Detection Limit of Entropy-Driven Catalytic DNA Circuit

The dual signal amplification resulting from the combination of release of many BDW and T strands using the CDC, and the multiple fluorophore labeled substrate on the SNA that the BDW will release, led to ultrasensitive detection of nucleic acid at a constant temperature (37 °C). To perform this experiment, BDW/S/W1 was annealed at a ratio of 1:2:4 (where initial [BDW]= 3μM). Following the annealing, the triplex BDW/S/W1 was diluted so that final [BDW] = 10nM and incubated with 40nM of F3 and varying concentration target DNA (see Table 1 for sequence) for 180 min at 37 °C. After incubation, 500pM F-Track SNA was added to the mixture in addition to 10 units nicking endonucleases. Fluorescence signals were measured immediately after adding the nicking enzyme. A dynamic range of 100 fM to 100 pM (Figure 25A) and a detection limit of 10 fM (Figure 25B) were achieved. As the sequences of T and BDW are completely decoupled, our strategy is universal and generalizable to any target nucleic acid with the same BDW and SNA.

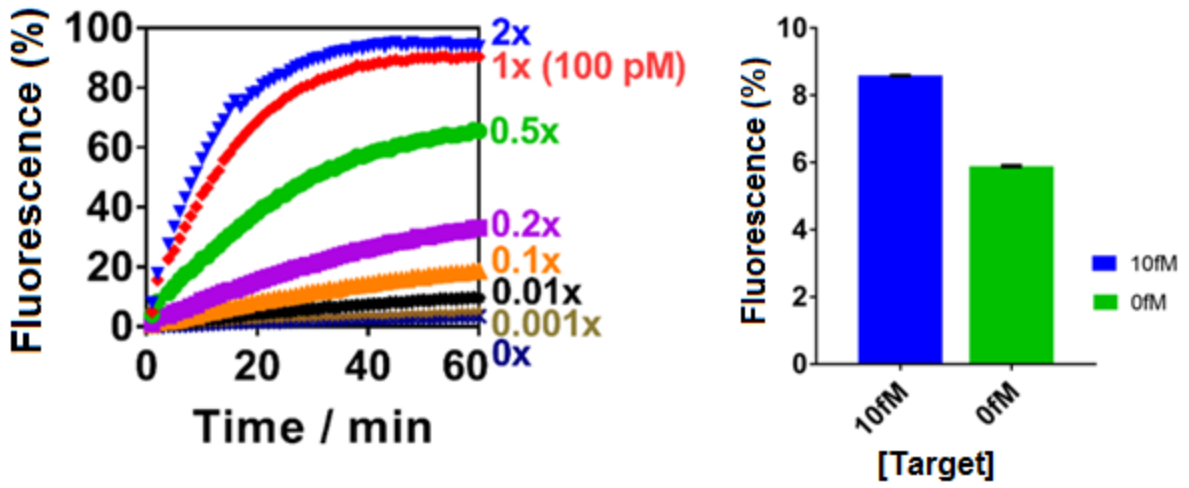

Figure 25. (A) Real-time monitoring the detection of target nucleic acid with concentrations varying from 100 fM to 200 pM. 1 × = 100 pM. (B) Detection limit of Target using the Entropy-Driven Catalytic-DNA-Circuit.

3.5 Rational Design of an Antibody Biosensor

We also engineered a BDW system for the detection of antibodies (Figure 26). Antibody-specific DNA nanodevices provide exciting opportunities for point-of-care disease diagnosis.[92-95] Our mechanistic study has revealed a new mechanism allowing the rapid, one-step, and amplified detection of antibodies or other proteins using stochastic DNA walkers. As our mechanistic study (Chapter 2, Section 2.2.3 Figure 10C) revealed that the BDW system is highly sensitive to steric hindrance at 3’ end, the detection of an antibody can be achieved by modifying a small molecular antigen at the 3’ end of BDW (Figure 26A). In this mechanism, the target antibody in solution will bind to the antigen on the 3' end of BDW. This large steric bulk created on the 3' end of BDW will then prevent the binding of the 3' foot of the BDW onto the F-Track. Since the 5' foot of BDW has a disfavoured orientation for binding, and the 3' foot is blocked by the antigen-antibody conjugate, BDW will only bind to the F-Track SNA slightly, releasing very

little fluorophore labeled substrate. Therefore, the presence of the antibody target should suppress any fluorescence signal generated by BDW walking on F-Track SNA. As a proof-of-concept, we chose the anti-biotin antibody as a model target and modified the BDW with biotin molecules. As shown in Figure 26C (red curve), the binding between the 3'-biotin and its antibody quantitatively deactivates the BDW, which generates a titration curve for the antibody with concentrations ranging from 100 pM to 100 nM. We also modified BDW with biotin labels at both 3' and 5' ends, to convert the BDW into a bidentate binder with enhanced affinity to its antibody (Figure 26B). Indeed, a higher sensitivity was observed for this construct (Figure 26C, blue curve). The activity in Figure 26, as well as in subsequent experiments is a normalized value of fluorescence signal generated by the free antigen-labeled BDW walking on the F-Track SNA and cleaving fluorophore labeled substrate. An activity of 1 is the same as 100% fluorescence shown in previous experiments.

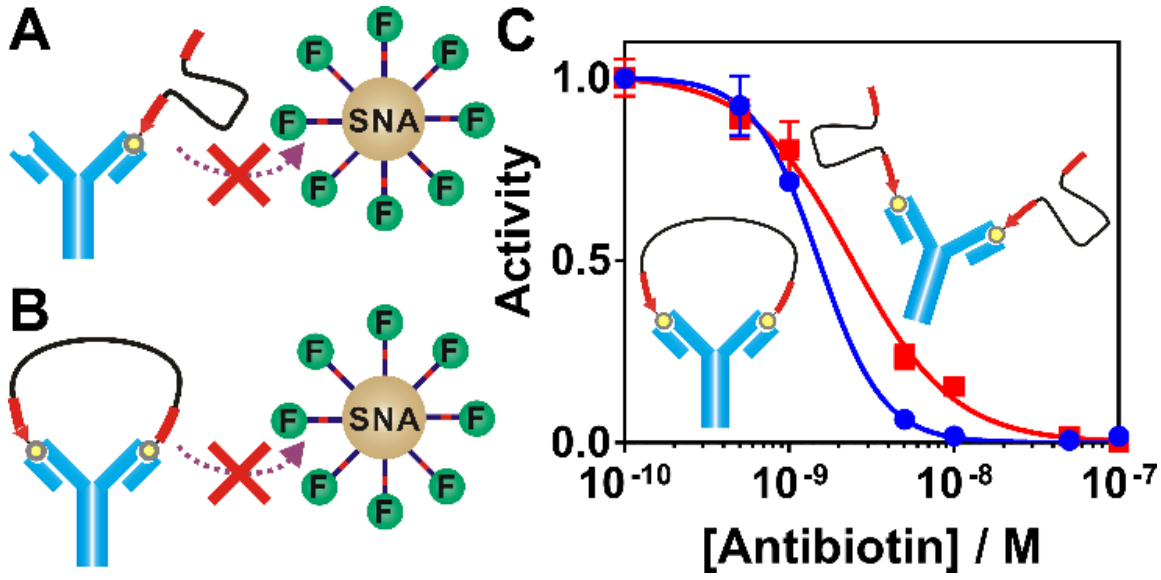

Figure 26. (A) Schematic illustration antibody-specific BDWs by modifying 3’ end with a biotin or (B) both 3’ and 5’ end with biotin molecules. (C) Titration curves of anti-biotin antibodies using single-biotin modified BDW (red) or dual biotin modified BDW (blue). Each error bar represent one standard deviation from triplicate analyses.

3.5.1 Optimization of the Antibody Biosensor

3.5.1.1 Feasibility of Biotin-labeled BDW as a DNA Walker

We used BDW-B, which is BDW functionalized with a biotin molecule on each of the 3' and 5' ends of its sequence, as the DNA walker to detect antibodies. As a proof-of-principle, BDW-B was compared to BDW. This was done by mixing either BDW or BDW-B with F-Track SNA, followed by the addition of the nicking endonuclease and measuring the fluorescence signal increase. As shown in Figure 27A, the BDW-B with biotin groups on the 3' and 5' end of BDW-B decrease the walking efficiency by around 30%. Testing the dynamic range of BDW-B, we

found that it has a dynamic range of 10nM to 100pM (Figure 27B). This was done by mixing varying concentration of BDW-B and incubating at 37 °C, followed by addition of 100pM F-Track SNA and nicking endonuclease and measuring fluorescence signal increase. As the concentration of BDW-B increased, the fluorescence signal observed increased. Therefore, BDW-B is a suitable DNA walker to use for protein detection.

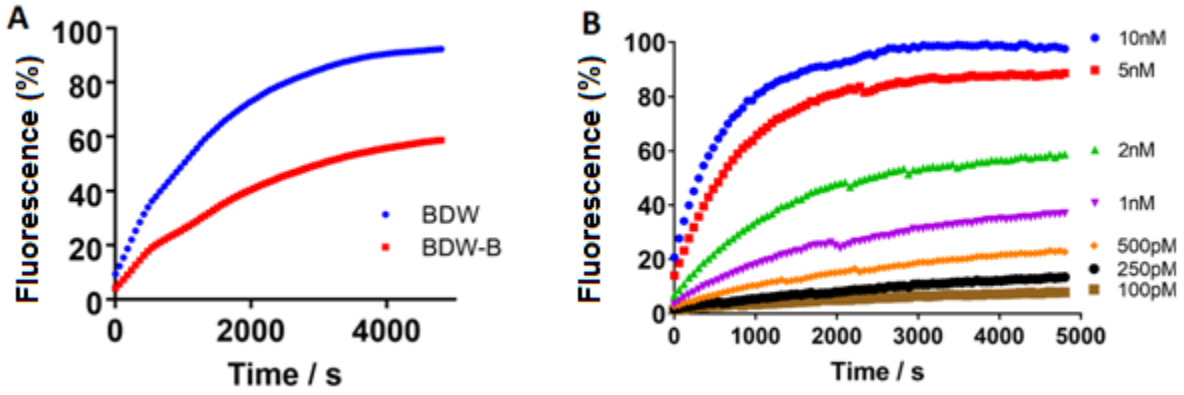

Figure 27. Testing the feasibility of BDW-B by comparing cleavage of substrate to BDW (A) (500pM = [BDW-B] = [BDW]. (B) Determining the dynamic range of BDW-B. Concentrations indicate [BDW-B] in solution.

3.5.1.2. Streptavidin Detection using BDW-B

As a proof-of-principle for detection of antibodies using BDW-B, we first explored the detection of streptavidin because streptavidin-biotin binding has a much greater affinity than anti-biotin-biotin, so in theory this combination should be the simplest system to explore if BDW-B has the ability to detect and quantify proteins. This was achieved by mixing 1nM of BDW-B with varying concentration of streptavidin and incubating for 30 min at 37 °C, followed by the addition of 100pM F-Track and nicking endonuclease, and measuring the fluorescence signal. The result of the streptavidin biosensor is shown in Figure 28. Figure 28A outlines the real-time

fluorescence monitoring of streptavidin detection using BDW-B. When using 100pM F-Track and 1nM BDW-B, 250pM of streptavidin could be detected in solution. As in Figure 26B, the detection of protein can be used to generate a titration curve for antibody with concentrations ranging from 10 nM to 10 pM (red curve, Figure 28B). The resulting titration curve has a steep slope which represents a very sensitive biosensor at the specific BDW-B concentration. Also in Figure 28B, we varied the concentration of both BDW-B and streptavidin in solution to compare the sensitivity of the biosensor at varying target concentration. We found that changing the BDW-B concentration had no impact on the sensitivity of our protein biosensor, which means we have the ability to tailor the protein detection platform to match specific target concentration ranges without sacrificing sensitivity. Finally, in Figure 28C, we compared the impact of using one biotin antigen on the 3' end of BDW-B vs. two antigen ligand, one on each foot of BDW-B. We found that the sensitivity of the dual-labeled BDW-B was greater than that of the single-labeled BDW-B (BDW-3'B). This is because BDW became a bidentate binder with enhanced affinity to the streptavidin target. However, because the binding affinity of biotin and streptavidin is very strong, the sensitivity difference is not as large as when single- and dual-labeled BDW-B was used for the detection of anti-biotin (Figure 26C).

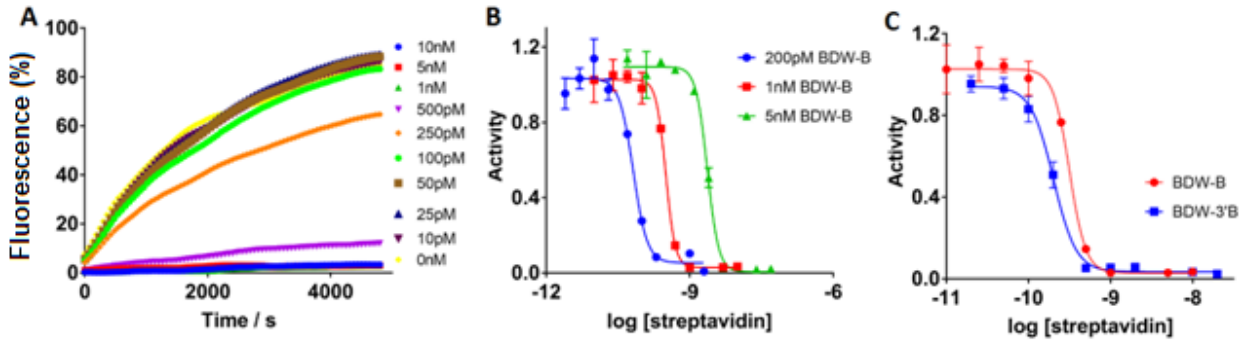

Figure 28. Detection of streptavidin using BDW-B. (A) Real-time fluorescence monitoring of BDW-B activity in the presence of varying [streptavidin]. (B) Titration curves for the detection of streptavidin using 200pM BDW-B (blue), 1nM BDW-B (red) and 5nM BDW-B. (C) Titration curve comparing the sensitivity of streptavidin detection using BDW-B with one biotin label on the 3' end (BDW-3'B) vs. using BDW-B with a biotin label on the 3' and 5' ends.

3.5.1.3 Anti-biotin Detection using BDW-B

We also used the dual-labeled BDW-B for detection of antibodies. Shown in Figure 26A-C was the mechanism of the biosensor for the detection of antibody followed by the comparison of one antigen label vs. two. To detect anti-biotin antibody, we mixed 1nM of BDW-B with varying concentration of anti-biotin and incubated the solution for 30 min at 37 °C, followed by the addition of 100pM F-Track and nicking endonuclease, then we measured the fluorescence signal increase. In Figure 29A&B, the real-time fluorescence data of anti-biotin detection using BDW-B is shown, followed by its titration curve. The biosensor had a detection limit of 1nM, and the titration curve generated showed less sensitivity than the titration curve for streptavidin detection, due to a weaker binding affinity between anti-biotin and biotin.

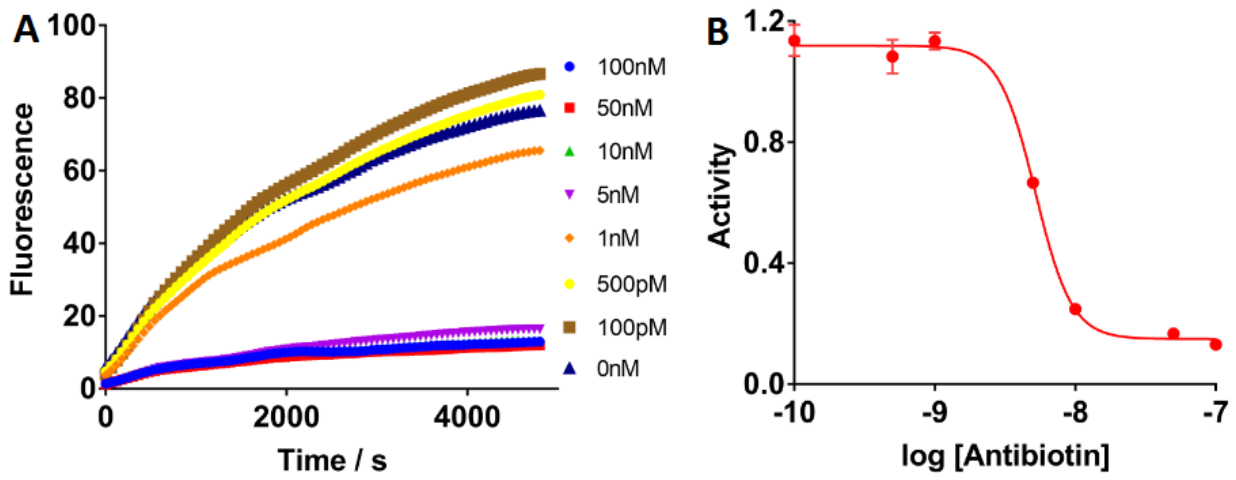

Figure 29. (A) Real-time fluorescence monitoring of anti-biotin detection using BDW-B (1nM BDW-B, 100pM F-Track). (B) Titration curve of anti-biotin detection using BDW-B.

3.5.1.4. Anti-digoxigenin Detection using BDW-D

Similarly to the anti-biotin detection, we also determined if BDW was able to detect anti-digoxigenin antibody in solution. This was achieved by modifying BDW to contain digoxin labeled on the 3' and 5' feet (BDW-D). BDW-D was mixed with varying concentrations of anti-digoxigenin and incubated for 30 min at 37 °C, followed by the addition of 100pM F-Track and nicking endonuclease. We then measured the fluorescence signal increase as a function of time. Figure 30 outlines the results. The performance of BDW-D consisted of a detection limit of 2.5 nM anti-digoxigenin, as well as a titration curve representing similar sensitivity to the anti-biotin detection. This result signifies that our BDW protein biosensor can be tuned by altering the antigens on each foot to detect many different antibodies, so long as the complement antigen is a small molecule (i.e. biotin and digoxin). These antigens are small enough to still enable the nicking recognition sites on BDW to hybridize to the nicking cleavage sites on the substrate on F-Track.

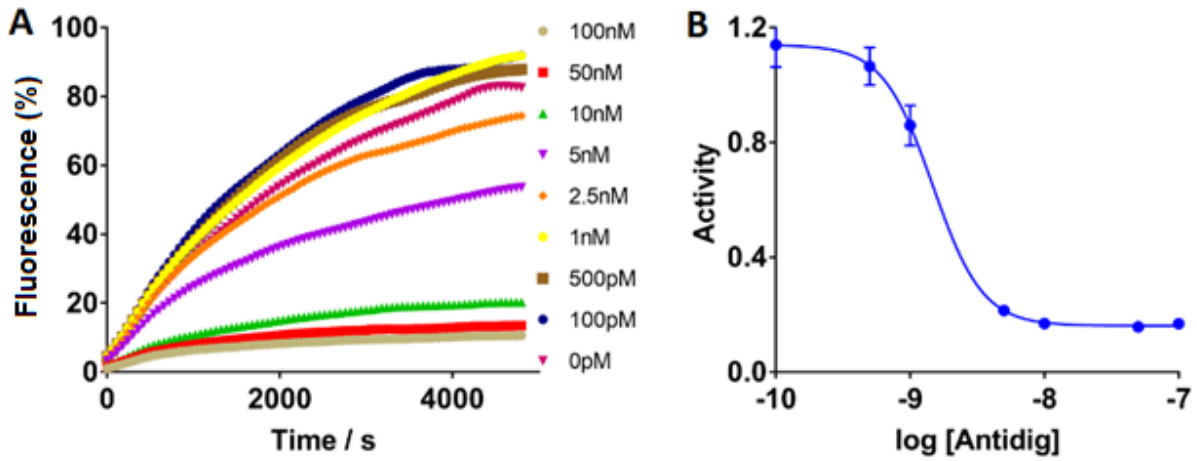

Figure 30. (A) Real-time fluorescence monitoring of anti-digoxigenin detection using BDW-B (1nM BDW-D, 100pM F-Track). (B) Titration curve of anti-dig detection using BDW-B.

3.6 Small Molecule Detection

Finally, we developed a biosensor that can detect small molecule targets in solution. This was achieved using BDW-B and F-Track as a signal generation and amplification components as well as anti-biotin to complete the biosensor. The biosensor is a competitive assay. This assay is a competitive assay in which the target biotin free in solution competes with the biotin on BDW-B to bind to the anti-biotin. We predict that when more free biotin is present in solution, less biotin on BDW-B should be able to bind to anti-biotin, resulting in a greater amount of BDW-B hybridizing to F-Track and cleaving the fluorophore-labeled substrate. Therefore, we can detect and quantify [biotin] in solution based on the fluorescence signal generated by BDW-B and F-Track (Figure 31A). We kept the concentration of BDW-B and anti-biotin constant (1 nM and 10 nM in the final solution, respectively), and varied free biotin concentration and measured fluorescence in real-time. The assay was performed by first mixing anti-biotin and the target biotin for 30 minutes at 37 °C. Following this incubation, BDW-B was added to the mixture, and

an additional 30 minute incubation at 37 °C was performed. Finally, 100pM F-Track and the nicking endonuclease was added to the solution and the fluorescence signal was monitored. The results are outlined in Figure 31B. We observed that as the concentration of biotin decreased, the fluorescence signal increased. This means that when more biotin was present in solution, it occupied the binding sites on the anti-biotin antibody, which allowed the BDW-B to bind to the F-Track SNA and cleave the fluorophore labeled substrate. We were able to detect 20nM biotin in solution after 30 min incubation and achieve a dynamic range from 1μM - 20nM.

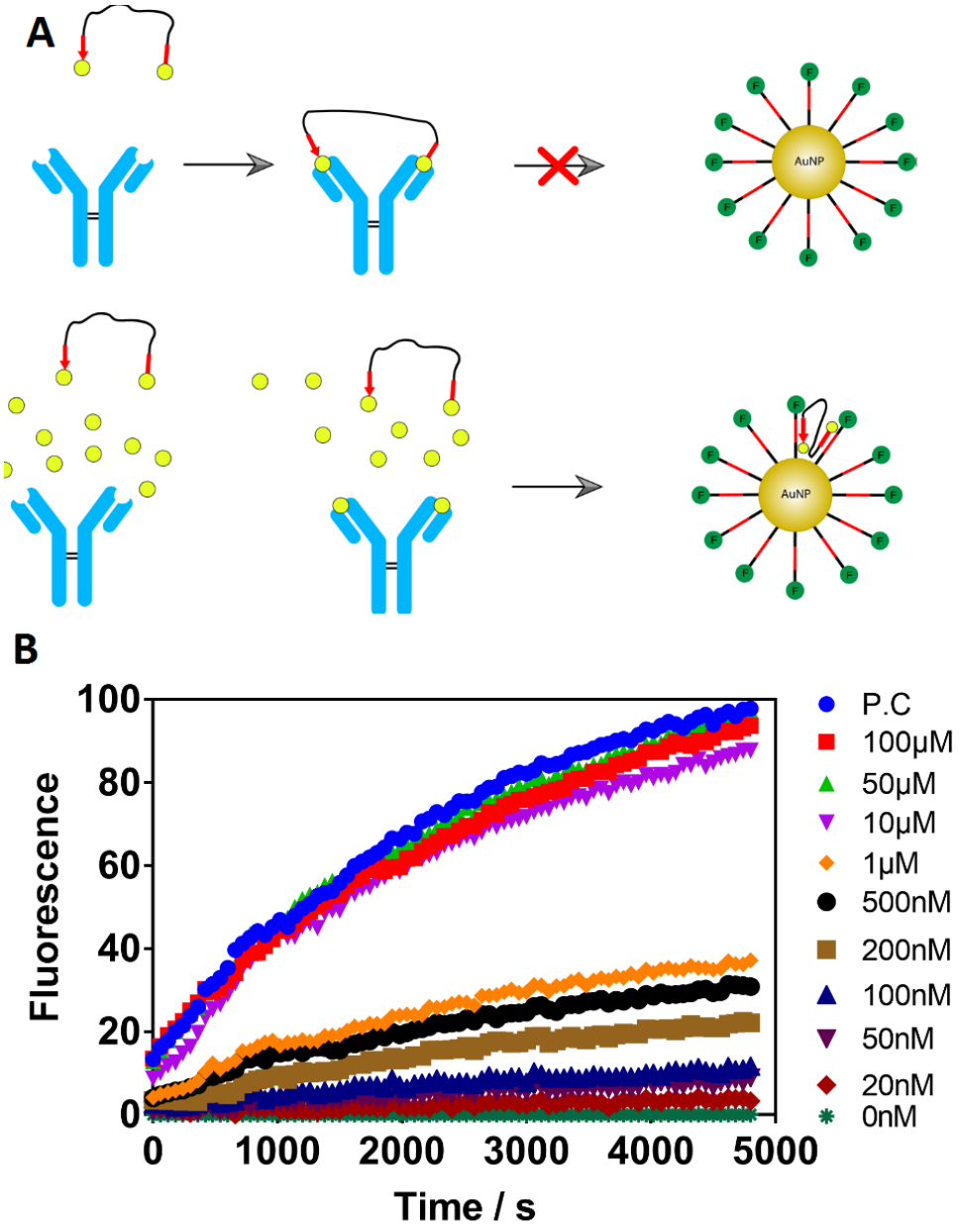

Figure 31. A) Schematic illustration of the small molecule detection platform. B) Dynamic range of biotin detection.

3.7 Conclusions

We have developed an approach to assemble a series of stochastic DNA walkers capable of probing and controlling dynamic interactions at bio-nano interfaces. By monitoring dynamics of these DNA walkers on SNA tracks, we have systematically investigated the effect of important interfacial factors, including intraparticle interaction, orientation, co-operativity, steric effect, multivalence, and binding hindrance, on enzymatic activities at the bio-nano interface. The improved understanding of these varying interfacial factors can be used for guiding the design and operation of biosensors and inspire new ideas and biosensing mechanisms. Our success in systemic probing dynamic interaction at bio-nano interfaces also demonstrates the new applications of dynamic DNA nanotechnology such as DNA walkers for addressing fundamental questions at the interface of chemistry and biology.

Chapter 4

Experimental Section

4.1 Chemicals and Materials.

All chemicals are of analytical grade and acquired from Sigma Aldrich (Oakville, ON, Canada) unless otherwise listed. 10000 units/mL Nb.BvCI and 10x Cutsmart Buffer were purchased from New England BioLabs (Whitby, ON, Canada). All DNA samples were purchased from Integrated DNA Technologies (Coralville, IA) and purified by high-performance liquid chromatography. The DNA sequences and modifications are listed in Table 1.

Table 1: DNA sequences and modifications

Note: Colour scheme represents DNA walker's feet/ nicking recognition sites and nicking cleavage sites on F-Track / T-Track DNA substrate (red), TDWs foot (blue), M-BDWs single base mutation (purple, underlined), fluorophore (light green, yellow), and complement regions in the CDC system between fuel, substrate, waste (light blue, green) and the target and substrate (light purple).

DNA Name		Sequences
DNA walkers	**BDW**	5'-CCT CAG CA CTG TGC GTG TGA CAT CCT CAG CA-3'
	TDW	5'-AAA AAA AAA AAA CTG TGC GTG TGA CAT CCT CAG CA-3'
	M-BDW	5'-CCT CAG CA CTG TGC GTG TGA CAT CCT CGG CAA-3'
	BDW-B (single label)	5'- CCT CAG CA CTG TGC GTG TGA CAT CCT CAG CA-**biotin**-3'
	BDW-B (dual label)	5'- **biotin** CCT CAG CA CTG TGC GTG TGA CAT CCT CAG CA-**biotin**-3'
	BDW-D (dual label)	5'- **digoxin-** CCT CAG CA CTG TGC GTG TGA CAT CCT CAG CA-**digoxin**-3'
	BDW-L1	5'-CCT CAG CAT CCT CAG CA-3'
	BDW-L6	5'-CCT CAG CA TTT TTT CCT CAG CA-3'
	BDW-L12	5'-CCT CAG CA TTT TTT TTT TTT CCT CAG

		CA-3'
	BDW9-L18	5'-CCT CAG CA TTT TTT TTT TTT TTT TTT CCT CAG CA-3'
	BDW9-L24	5'-CCT CAG CA TTT TTT TTT TTT TTT TTT TTT TTT CCT CAG CA-3'
	3'SDW	5'- CTG TGC GTG TGA CAT CCT CAG CAA-3'
	5'SDW	5'-CCT CAG CAA CTG TGC GTG TGA CAT -3'
SNA Track	**F-Track**	5'-SH-T TTT TTT TTT GC*T GAG GAT-FAM-3' (*cleavage site)
	T-Track	5'- SH-T TTT TTT TTT GC*T GAG GAT-TAMRA-3' (*cleavage site)
Protecting DNA for BDW	**3' Protection (for BDW)**	5'- TGA GG ATGT CAC ACG CAC AG-3'
	5' Protection (for BDW)	5'- ATGT CAC ACG CAC AG TGCTG -3'
	Dual Protection	5'- TGA GG ATGT CAC ACG CAC AG TGCTG -3'
	Probe for duplex spacer	5'- ATGT CAC ACG CAC AG -3'
Entropy-driven catalytic DNA circuit	**Substrate (S)**	5'- CTG AGG ATG TCA CAC GCA CAG TGC TGA AGTCT CGC CAA TAT TTA CGT GCT GCT A -3'
	Waste-1 (W1)	5'- ACG TAA ATA TTG GCG AGA CT -3'
	Fuel-1 (F1)	5'- ACG TAA ATA TTG GCG AGA CT TCAGCA C TGT GCG TGT GAC AT C CTC AG -3'
	Fuel-2 (F2)	5'- ACG TAA ATA TTG GCG AGA CT TCAGCA C TGT GCG TGT GAC AT C CTC -3'
	Fuel-3 (F3)	5'- ACG TAA ATA TTG GCG AGA CT TCAGCA C TGT GCG TGT GAC AT -3'
	Target (T)	5'-TAG CAG CAC GTA AAT ATT GGCG-3'

4.2 Preparation and Characterization of SNA Tracks.

Preparation of the SNA track was achieved by conjugating functional DNA probes onto gold nanoparticles according our previously established method[23]. Typically, substrate oligonucleotides were mixed at a concentration of 50 μM with 500 μL of 1 nM AuNPs. This mixture was incubated at room temperature for 12 h and then was slowly mixed with 16.5 μL of 3 M NaCl, followed by 10 s of sonication. This process of addition of NaCl and sonication was

repeated five times with a 1 h interval to maximize the oligonucleotide loading amounts[24]. The solution was then incubated at room temperature for 24 h. After incubation, the solution was centrifuged at 14 000 rpm for 30 min to separate the DNA-functionalized AuNPs (SNAs) from the unreacted reagents. The DNA−AuNPs were washed three times with 1× PBS buffer (pH 7.4) containing 0.01% Tween 20 and finally redispersed in PBS buffer. After preparation, fluorescence spectroscopy was used to determine the coverage of substrate oligonucleotides on each AuNP. This was determined by releasing substrate from AuNP using 45 mM DTT and measuring fluorescence of the FAM dye that was labeled on substrate[25]. Fluorescence was measured using a multimode microplate reader (SpectraMax i3, Molecular Devices), and F-Track substrate coverage was quantified by using FAM-labeled F-Track substrate oligos as external standards.

4.3 Real-Time Monitoring DNA Walkers on SNA Tracks.

For a typical BDW reaction on SNA track, a reaction mixture containing 500 pM BDW, 500pM F-Track SNA, 10 units nicking endonucleases, and 1× NEB CutSmart buffer was added to a 96-well microplate. Fluorescence signals were measured immediately after adding the nicking enzyme. This measurement was carried out at 37 °C measuring signal increase every 1 min using a multimode microplate reader with excitation/ emission wavelength of 485/535 nm to monitor the released FAM-labeled substrate.

4.4 Design and Application of DNA-Walker based Biosensors for the Detection of Nucleic Acids, Proteins and Small Molecules

4.4.1 Detection of Nucleic Acids.

The procedure for detection of nucleic acids using the nucleic acid biosensor begins with hybridization of 3 μM BDW with a long single stranded scaffold DNA strand (Substrate (S), see Table 1 for sequence) and a additional short single stranded protecting sequence (W1, see Table 1 for sequence) through an annealing process at a 1:2:4 ratio BDW:S:W1. The resulting triplex DNA structure was diluted and mixed with a 40x concentrated fuel DNA strand (F, see Table 1 for sequence) and target DNA (T, see Table 1 for sequence) and incubated at 37 °C for 3 hrs. Reaction mixture was mixed with 500pM F-Track SNA, 10 units nicking endonucleases, and 1× NEB CutSmart buffer. Fluorescence signals were measured immediately after adding the nicking enzyme. This measurement was carried out at 37 °C in a 96-well microplate, measuring signal increase every 1 min using a multimode microplate reader with excitation/ emission wavelength of 485/535 nm to monitor the released FAM-labeled substrate.

4.4.2 Detection of Antibodies.

The procedure for detection of antibodies using the protein biosensor begins with incubation of 10nM antigen-functionalized BDW and anti-biotin antibodies for 30 min at 37 °C in a T100 Thermal cycler. Reaction mixture was mixed with 500pM F-Track SNA, 10 units nicking endonucleases, and 1× NEB CutSmart buffer. Fluorescence signals were measured immediately after adding the nicking enzyme. This measurement was carried out at 37 °C in a 96-well microplate, measuring signal increase every 1 min using a multimode microplate reader with excitation/ emission wavelength of 485/535 nm to monitor the released FAM labeled substrate.

4.4.3 Detection of Small Molecules.

The procedure for detection of small molecules using the protein biosensor begins with incubation of 1nM antigen-functionalized BDW 10nM anti-biotin antibodies as well as biotin for

30 min at 37 °C in a T100 Thermal cycler. Reaction mixture was mixed with 100pM F-Track SNA, 10 units nicking endonuclease, and 1× NEB CutSmart buffer. Fluorescence signals were measured immediately after adding the nicking enzyme. This measurement was carried out at 37 °C in a 96-well microplate, measuring signal increase every 1 min using a multimode microplate reader with excitation/ emission wavelength of 485/535 nm to monitor the released FAM labeled substrate.

4.4.4 Data Normalization for experiments

In a typical test, BDW and F-Track were pre-incubated and monitored in a microplate reader for 10 min before adding nicking endonuclease (10 U) at 0 min. After plate reading, the signal from the negative control (containing only F-Track and nicking enzyme) was subtracted from all other signals in order to normalize signals, avoiding day-to-day fluctuation in fluorescence signal readout obtained from the spectrophotometer.

Chapter 5

Conclusions and Future Work

We demonstrated an approach to assemble a series of stochastic DNA walkers capable of probing dynamic interactions occurring at the bio-nano interface. By monitoring dynamics of DNA walkers on spherical nucleic acid (SNA) tracks, we systematically investigated effects of varying interfacial factors, including intramolecular interactions, orientation, co-operativity, steric effect, multivalence, and binding hindrance on enzymatic activities at the bio-nano interface. The knowledge we gained was then applied to fabricate ultrasensitive biosensors for amplified detection of nucleic acids and antibodies. The result of our work both furthers the emerging applications of DNA walkers, but meanwhile illustrates that a biosensor system using a DNA walker and a 3D track contains a critical interface that needs to be better understood, as properties realized can be used to optimize the biosensor. Our study revealed critical roles of interfacial factors to enzyme activities and performance of enzyme-driven nanodevices. We also demonstrate that improvement in understanding bio-nano interfaces will facilitate the design and operation of biosensors and inspire new sensing mechanisms.

Future work in this field could consist of using the TDW (Chapter 2, Figure 8) or other similar DNA walkers to explore the bio-nano interface to determine if any of the established critical factors at the interface, such as valence, binding hindrance, adsorption, orientation, and curvature effects, need can be changed to optimize walking performance and biosensor development. Additionally, we need to explore more diverse DNA walker designs, such as a bipedal walker tethered to the SNA track or multipedal walkers, to find DNA walkers with improved binding affinity, faster walking speeds and sensitive biosensors. For example, given the difference in

catalytic efficiency of the 3' and 5' foot of BDW, developing a DNA walker to contain two 3' feet through hybridization of two 3'SDWs could present a solution to the decreased catalytic efficiency of the 5' foot of BDW. Additionally, using two types of substrate functionalized to the AuNP track could solve this issue as well. The two types of substrate would have opposite polarity to each other, in such a way that each foot of BDW can hybridize to them the was 3' foot hybridizes to the substrate in the current designs.

References

[1] Watson, J. D.; Crick, F. H. Genetical Implications of the Structure of Deoxyribonucleic Acid. *Nature*. **1953**, 171, 964–967.

[2] Alberts, B.; Bray, D.; Hopkin, K.; Johnson, A.; Lewis, J.; Raff, M.; Walter, P. (2013). *Essential cell biology*. Garland Science.

[3] Wilkins, M. H. F.; Stokes, A. R.; Wilson, H. R. Molecular Structure of Nucleic Acids: Molecular Structure of Deoxypentose Nucleic Acids. *Nature,* **1953**, 171, 738-740.

[4] Horton, H. R.; Moran, L. A.; Ochs, R. S.; Rawn, J. D.; Scrimgeour, K. G. *Principles of Biochemistry*, 3rd ed.; Prentice Hall: Upper Saddle River, NJ, **2002**.

[5] Bartels, C. L.; Tsongalis, G. J. MicroRNAs: novel biomarkers for human cancer. *Clinical Chemistry* **2009**, 55, 623-631.

[6] Mason, S.; Tang, Y.; Li, Y.; Xie, X.; Li, F. Emerging bioanalytial applications of DNA walkers. *Trends in Analytical Chemistry* **2018**, 107, 212-221.

[7] Soriano, M. L.; Zougagh, M.; Valcarcel,M.; Rios, A. Analytical nanoscience and nanotechnology: where we are and where we are heading. *Talanta* **2018**, 177, 104-121.

[8] Zhang, D. Y.; Seelig, G. Dynamic DNA nanotechnology using strand-displacement reactions. *Nat. Chem* **2011,** 3, 103-113.

[9] Chao, J.; Zhu, D.; Zhang, Y.; Wang, L.; Fan, C. DNA nanotechnology-enabled biosensors. *Biosens. Bioelectron*. **2016**, 76, 68-79.

[10] Hong, F.; Zhang, F.; Liu, Y.; Yan, H. DNA origami: scaffolds for creating higher order structures. *Chem. Rev.* **2017**, 117, 12584-12640.

[11] Bath, J.; Turberfield, A. J. DNA nanomachines. *Nat. Nanotechnol*. **2007**, 2, 275-284.

[12] Jung, C.; Ellington, A. D. Diagnostic applications of nucleic acid circuits. *Acc. Chem. Res.* **2014**, 47, 1825-1835.

[13] Wang, F.; Liu, X.; Willner, I. DNA switches: from principles to applications. *Angew. Chem. Int. Ed.* **2015**, 54, 1098-1129.

[14] Dirks, R. M.; Pierce, N. A. Triggered amplification by hybridization chain reaction. *Proc. Natl. Acad. Sci. U. S. A.* **2004**, 101, 15275-15278.

[15] Li, B.; Ellington, A. D.; Chen, X. Rational, modular adaptation of enzyme-free DNA circuits to multiple detection methods. *Nucleic Acids Res.* **2011**, 39, e110.

[16] Zhang, D. Y.; Turberfield, A. J.; Yurke, B.; Winfree, E. Engineering entropy-driven reactions and networks catalyzed by DNA. *Science* **2007**, 318, 1121-1125.

[17] Chen, X. Expanding the Rule Set of DNA Circuitry with Associative Toehold Activation. *J. Am. Chem. Soc.* **2012**, 134, 263–271.

[18] Li, F.; Zhang, H.; Wang, Z.; Li, X.; Li, X. F.; Le, X. C. Dynamic DNA Assemblies Mediated by Binding-Induced DNA Strand Displacement. *J. Am. Chem. Soc.* **2013**, 135, 2443–2446.

[19] Zhang, D. Y.; Turberfield, A. J.; Yurke, B.; Winfree, E. Engineering Entropy-Driven Reactions and Networks Catalyzed by DNA. *Science* **2007**, 318, 1121–1125.

[20] Zhang, D. Y.; Winfree, E. Control of DNA strand displacement kinetics using toehold exchange. *J. Am. Chem. Soc.* **2009**, 131, 17303-17314.

[21] Zhang, D. Y.; Chen, S. X.; Yin, P. Optimizing the specificity of nucleic acid hybridization. *Nat. Chem.* **2012**, 4, 208-214.

[22] Wang, J. S.; Zhang, D. Y. Simulation-guided DNA probe design for consistently ultraspecific hybridization. *Nat. Chem.* **2015**, 7, 545-553.

[23] Zhang, H.; Li, F.; Dever, B.; Wang, C.; Li, X.-F.; C. Le, X. C. Assembling DNA through affinity binding to achieve ultrasensitive protein detection. *Angew. Chem. Int. Ed.* **2013**, 52, 10698-10705.

[24] Li, F.; Lin, Y.; Le, X. C. Binding-induced formation of DNA three-way junctions and its application in real-time protein detection and DNA strand displacement. *Anal. Chem.* **2013**, 85, 10835-10841.

[25] Tang, Y.; Wang, Z.; Yang, X.; Chen, J.; Liu, L.; Zhao, W.; Le, X. C.; Li, F. Constructing real-time, wash-free, and reiterative sensors for cell surface proteins using binding-induced dynamic DNA assembly. *Chem. Sci.* **2015**, 6, 5729-5733.

[26] Tang, Y.; Lin, Y.; Yang, X.; Wang, Z.; Le, X. C.; Li, F. Universal strategy to engineer catalytic DNA hairpin assemblies for protein analysis. *Anal. Chem.* **2015**, 87, 8063-8066.

[27] Pan, J.; Li, F.; Cha, T. G.; Choi, J. H. Recent progress on DNA based walkers. *Curr. Opin. Biotechnol.* **2015**, 34, 56-64.

[28] Delius, M. V.; Leigh, D. A.Walking molecules. *Chem. Soc. Rev.*, **2011**, 40, 3656-3676.

[29] Xing, Y.; Liu, B.; Chao, J.; Wang, L. DNA-based nanoscale walking devices and their applications. *RSC Adv.* **2017**, 7, 47425.

[30] Soleymani, L.; Li, F. Mechanistic challenges and advantages of biosensor miniaturization into the nanoscale. *ACS Sens.* **2017**, 2, 458-467.

[31] Thubagere, A. J.; Li, W.; Johnson, R. F.; Chen, Z.; Doroudi, S.; Lee, Y. L.; Izatt, G.; Wittman, S.; Srinivas, N.; Woods, D.; Wingree, E.; Qian, L. A cargo-sorting DNA robot. *Science* **2017**, 357, eaan6558.

[32] Jung, C.; Allen, P. B.; Ellington, A. D. A stochastic DNA walker that traverses a microparticle surface. *Nat. Nanotechnol.* **2016**, 11, 157-163.

[33] Rothemund, P. W. K. Folding DNA to create nanoscale shapes and patterns. *Nature*. **2006**, 440, 297-302.

[34] Tian, Y.; He, Y.; Chen, Y.; Yin, P.; Mao, C. A DNAzyme that walks processively and autonomously along a one-dimensional track. *Angew. Chem. Int. Ed.* **2005**, 44, 4355-4358.

[35] Pei, R.; Taylor, S. K.; Stefanovic, D.; Rudchenko, S.; Mitchell, T. E.; Stojanovic, M .N. Behavior of Polycatalytic Assemblies in a Substrate-Displaying Matrix. *J. Am. Chem. Soc.* **2006**, 128, 12693-12699.

[36] Lund, K.; Manzo, A. J.; Dabby, N.; Michelotti, N.; Johnson-Buck, A.; Nangreave, J.; Taylor, S.; Pei, R.; Stojanovic, M. N.; Walter, N. G.; Winfree, E.; Yan, H. Molecular robots guided by prescriptive landscapes. *Nature* 465, **2010**, 465, 206-209.

[37] Bath, J.; Green, S. J.; Turberfield, A. J. A free-running DNA motor powered by a nicking enzyme. *Angew. Chem. Int. Ed.* **2005**, 44, 4358-4361.

[38] Yang, X.; Tang, Y.; Mason, S. D.; Chen, J.; Li, F. Enzyme-powered three-dimensional DNA nanomachine for DNA walking, payload release, and biosensing. *ACS Nano* **2016**, 10, 2324-2330.

[39] Qu, X.; Zhu, D.; Yao, G.; Su, S.; Chao, J.; Liu, H.; Zuo, X.; Wang, L.; Shi, J.; Wang, L.; Huang, W.; Pei, H., Fan C. An exonuclease III-powered, on-particle stochastic DNA walker. *Angew. Chem. Int. Ed.* **2017**, 56, 1855-1858.

[40] Yehl, K.; Mugler, A.; Vivek, S.; Liu, Y.; Zhang, Y.; Fan, M.; Weeks, E. R.; Salaita, K. High-speed DNA-based rolling motors powered by RNase H. *Nat. Nanotechnol.* **2016**, 11, 184-190.

[41] You, M.; Chen, Y.; Zhang, X.; Liu, H.; Wang, R.; Wang, K.; Williams, K. R. Tan, W. An autonomous and controllable light-driven DNA walking device. *Angew. Chem. Int. Ed.* **2012**, 51, 2457-2460.

[42] Sherman, W. B.; Seeman, N. C. A Precisely controlled DNA biped walking device. *Nano Lett.* **2004**, 4, 1203-1207.

[43] Wang, L.; Deng, R.; Li, J. Target-fueled DNA walker for highly selective miRNA detection. *Chem. Sci.* **2015**, 6, 6777-6782.

[44] Peng, L.; Zhang, P.; Chai, Y.; Yuan, R. Bi-directional DNA walking machine and its application in an enzyme-free electrochemiluminescence biosensor for sensitive detection of microRNAs. *Anal. Chem.* **2017**, 89, 5036-5042.

[45] Chen, Y.; Xiang, Y.; Yuan, R.; Chai, Y. A restriction enzyme-powered autonomous DNA walking machine: its application for a highly sensitive electrochemiluminescence assay of DNA. *Nanoscale* **2015**, 7, 981-986.

[46] Wang, D.; Vietz, C.; Schroder, T.; Acuna, G.; Lalkens, B.; Tinnefeld, P. A DNA walker as a fluorescence signal amplifier. *Nano Lett.* **2013**, 17, 5368-5347.

[47] Li, C.; Li, X.; Wei, L.; Liu, M.; Chen, Y.; Li, G. Simple electrochemical sensing of attomolar proteins using fabricated complexes with enhanced surface binding avidity. *Chem. Sci.* **2015**, 6, 4311-4317.

[48] Ji, C.; Zhang, L.; Zhu, L.; Lei, J.; Wu, J.; Ju, H. Binding-induced DNA walker for signal amplification in highly selective electrochemical detection of protein. *Biosens. Bioelectron.* **2017**, 96, 201-205.

[49] Cai, S.; Chen, M.; Liu, M.; He, W.; Liu, Z.; Wu, D.; Xia, Y.; Yang, H.; Chen, J. A signal amplification electrochemical aptasensor for the detection of breast cancer cell via free-running DNA walker. *Biosens. Bioelectron.* **2016**, 85, 184-189.

[50] Zhu, L.; Liu, Q.; Yang, B.; Ju, H.; Lei, J. Pixel counting of fluorescence spots triggered by DNA walkers for ultrasensitive quantification of nucleic acid. *Anal. Chem.* **2018**, 90, 6357-6361.

[51] Jung, C.; Allen, P. B.; Ellington, A. D.; A simple, cleated DNA walker that hands on to surfaces. *ACS Nano* **2017**, 11, 8047-8054.

[52] Li, W.; Wang, L.; Jiang, W. A catalytic assembled enzyme-free three-dimensional DNA walker and its sensing application. *Chem. Commun.* **2017**, 53, 5527-5530.

[53] Li, N.; Zheng, J.; Li, C.; Wang, X.; Ji, X.; He, Z. An enzyme-free DNA walker that moves on the surface of functionalized magnetic microparticles and its biosensing analysis. *Chem. Commun.* **2017**, 53, 8486-8488.

[54] Jiang, X.; Wang, H.; Wang, H.; Zhuo, Y.; Yuan, R.; Chai, Y. Electrochemiluminescence biosensor based on 3-D DNA nanomachine signal probe powered by protein-aptamer binding complex for ultrasensitive mucin 1 detection. *Anal. Chem*. **2017**, 89, 4280-4286.

[55] He, M.-Q.; Wang, K.; Wang, W.-J.; Yu, Y.-L.; Wang, J.-H. Smart DNA machine for carcinoembryonic antigen detection by exonuclease III-assisted target recycling and DNA walker cascade amplification. *Anal. Chem.* **2017**, 89, 9292-9298.

[56] Zhang, Y.; Wang, L.; Luo, F.; Qiu, B.; Guo, L.; Weng, Z.; Lin, Z.; Chen, G. An electrochemiluiminescence biosensor for Kras mutations based on locked nucleic acid functionalized DNA walker and hyperbranched rolling circle amplification. *Chem. Commun.* **2017**, 53, 2910-2913.

[57] Xu, Z.; Liao, L.; Chai, Y.; Wang, H.; Yuan, R. Ultrasensitive electrochemiluminescence biosensor for microRNA detection by 3D DNA walking machine based target coversion and distance-controllable signal quenching and enhancing. *Anal. Chem.* **2017**, 89, 8282-8287.

[58] Zhang, H.; Lai, M.; Zuehlke, A.; Peng, H.; Li, X.-F.; Le, X. C. Binding-induced DNA nanomachines triggered by proteins and nucleic acids. *Angew. Chem. Int. Ed.* **2015**, 127, 14534-14538.

[59] Chen, J.; Zuehlke, A.; Deng, B.; Peng, H.; Hou, X.; Zhang, H. A target-triggered DNAzyme motor enabling homogeneous amplified detection of proteins. *Anal. Chem.* **2017**, 89, 12888-12895.

[60] Li, F.; Zhang, H.; Lai, C.; Li, X.-F.; Le, X. C. Molecular translator that acts by binding-induced DNA trand displacement for a homogeneous protein assay. *Angew. Chem. Int. Ed.* **2012**, 51, 9317-9320.

[61] Li, F.; Lin, Y.; Lau, A.; Tang, Y.; Chen, J.; Le, X. C. Binding-induced molecular amplifier as a universal detection platform for biomolecules and biomolecular interaction. *Anal. Chem.* **2018**, 90, 8651-8657.

[62] Rosi, N. L.; Giljohann, D. A.; Thaxton, C. S.; Lytton-Jean, A. K.; Han, M. S.; Mrikin, C. A. Oligonucleotide-modified gold nanoparticles for intracellular gene regulation. *Science* **2006**, 312, 1027-1030.

[63] Peng, H.; Li, X.-F.; Zhang, H.; Le, X. C. A microRNA-initiated DNAzyme motor operating in living cells. *Nat. Commun.* **2017**, 8, 14378.

[64] Liang, C.-P.; Ma, P. Q.; Liu, H.; Guo, X.; Yin, B.-C.; Ye, B.-C. Rational engineering of a dynamic, entropy-driven DNA nanomachine for intracellular microRNA imaging. *Angew. Chem. Int. Ed.* **2017**, 56, 9077-9081.

[65] Ma, P.-Q.; Liang, C.-P.; Zhang, H-H.; Yin, B.-C.; Ye, B.-C. A highly integrated DNA nanomachine operating in living cells powered by an endogenous stimulus. *Chem. Sci.* **2018**, 9, 3299-3304.

[66] You, M.; Lyu, Y.; Han, D.; Qiu, L.; Liu, Q.; Chen, T.; Wu, C.; Peng, L.; Zhang, L.; Bao, G.; Tan, W. A DNA probe for monitoring dynamic and transient molecular encounters on live cell membranes. *Nat. Nanotechnol.* **2017**, 12, 453-459.

[67] Li, J.; Johonson-Buck, A.; Yang, Y. R.; Shih, W. M.; Yan, H.; Walter, N. G. Exploring the speed limit of toehold exchange with a cartwheeling DNA acrobat. *Nat. Nanotechnol.* **2018**, 13, 723-729.

[68] Bui, H.; Shah, S.; Mokhtar, R.; Song, T.; Garg, S.; Reif, J. Localized DNA hybridization chain reactions on DNA origami. *ACS Nano* **2018**, 12, 1146-1155.

[69] Mason, S. D.; Wang, G. A.; Yang, P.; Li, Y.; Li, F. Probing and controlling dynamic interactions at biomolecule-nanoparticle interfaces using stochastic DNA walkers. *ACS Nano*, **2019**, *13*, 8106-8113.

[70] Rosi, N. L.; Mirkin, C. A. Nanostructures in Biodiagnostics. *Chem. Rev.* **2005**, 105, 1547-1562.

[71] Farka, Z.; Jurik, T.; Kovar, D.; Trnkova, L.; Skladal, P. Nanoparticle-based Immunochemical Biosensors and Assays: Recent Advances and Challenges. *Chem. Rev.* **2017**, 117, 9973-10042.

[72] Saha, K.; Agasti, S. S.; Kim, C.; Li, X.; Rotello, V. M. Gold Nanoparticles in Chemical and Biological sensing. *Chem. Rev.* **2012**, 112, 2739-2779.

[73] Rosi, N. L.; Giljohann, D. A.; Thaxton, C. S.; Lytton-Jean, A. K. R.; Han, M. S.; Mirkin, C. A. Oligonucleotide-Modified Gold Nanoparticles for Intracellular Gene Regulation. *Science* **2006**, 312, 1027–1031.

[74] Chen, G.; Roy, I.; Yang, C.; Prasad, P. N. Nanochemistry and nanomedicine for nanoparticle-based diagnostics and therapy. *Chem. Rev.* **2016**, 116, 2826-2885.

[75] Willner, I.; Willner, B. Biomolecule-Based Nanomaterials and Nanostructures. *Nano Lett.* **2010**, 10, 3805–3815.

[76] Gao, J.; Gu, H.; Xu, B. Multifunctional Magnetic Nanoparticles : Design , Synthesis , and Biomedical Applications. *Acc. Chem. Res.* **2009**, 42, 1097–1107.

[77] Erathodiyil, N.; Ying, J. Y. Functionalization of Inorganic Nanoparticles for Bioimaging Applications. *Acc. Chem. Res.* **2011**, 44, 925–935.

[78] Algar, W. R.; Jeen, T.; Massey, M.; Peveler, W. J.; Asselin, J. Small Surface, Big Effects, and Big Challenges: Toward Understanding Enzymatic Activity at the Inorganic Nanoparticle − Substrate Interface. *Langmuir* **2019**, 35, 7067-7091.

[79] Johnson, B. J.; Algar, W. R.; Malanoski, A. P.; Ancona, M. G.; Medintz, I. L. Understanding Enzymatic Acceleration at Nanoparticle Interfaces: Approaches and Challenges. *Nano Today* **2014**, 9, 102−131.

[80] Hill, H. D.; Millstone, J. E.; Banholzer, M. J.; Mirkin, C. A. The Role Radius of Curvature Plays in Thiolated Oligonucleotide Loading on Gold Nanoparticles. *ACS Nano*, **2009**, 3, 418–424.

[81] Liu, L.; Xu, K.; Wang, H.; Tan, P. K.; Fan, W.; Venkatraman, S. S.; Li, L.; Yang, Y. Y. Self-Assembled Cationic Peptide Nanoparticles as an Efficient Antimicrobial Agent. *Nat. Nanotechnol.* **2009**, 4, 457-463.

[82] Vranish, J. N.; Ancona, M. G.; Walper, S. A.; Medintz, I. L. Pursuing the Promise of Enzymatic Enhancement with Nanoparticle Assemblies. *Langmuir* **2018**, 34, 2901−2925

[83] Algar, W. R.; Malonoski, A.; Deschamps, R.; Blanco-canosa, J. B.; Susumu, K.; Stewart, M. H.; Johnson, B. J.; Dawson, P. E.; Medintz, I. L. Proteolytic Activity at Quantum Dot-Conjugates: Kinetic Analysis Reveals Enhanced Enzyme Activity and Localized Interfacial "Hopping". *Nano Lett.* **2012**, 12, 3793–3802.

[84] Seferos, D. S.; Prigodich, A. E.; Giljohann, D. A.; Patel, P. C.; Mirkin, C. A. Polyvalent DNA Nanoparticle Conjugates Stabilize Nucleic Acids. *Nano Lett.* **2009**, 9, 308–311.

[85] Prigodich, A. E.; Alhasan, A. H.; Mirkin, C. A. Selective Enhancement of Nucleases by Polyvalent DNA-Functionalized Gold Nanoparticles. *J. Am. Chem. Soc.* 2011, *133*, 2120–2123.

[86] Li, Y.; Wang, G, A.; Mason, S. D.; Yang, X.; Yu, Z.; Tang, Y.; Li, F. Simulation-guided engineering of an enzyme-powered three dimensional DNA nanomachine for discriminating single nucleotide variants. *Chem. Sci.* **2018**, 9, 6434-6439.

[87] Li, F.; Zhang, H.; Dever, B.; Li, X.-F.; Le, X. C. Thermal Stability of DNA Functionalized Gold Nanoparticles. *Bioconjugate Chem*. **2013**, 24, 1790−1797.

[88] Hurst, S. J.; Lytton-Jean, A. K.; Mirkin, C. A. Maximizing DNA Loading on a Range of Gold Nanoparticle Sizes. *Anal. Chem.* **2006**, 78, 8313−8318.

[89] Swift, J. L.; Cramb, D. T. Nanoparticles as Fluorescence Labels: Is Size All that Matters? *Biophysical Journal* **2008,** 95, 865-876.

[90] Kuzuya, A.; Numajiri, K.; Kimura, M.; Komiyama M. Single-Molecule Accommodation of Streptavidin in Nanometer-Scale Wells Formed in DNA Nanostructures. *Nucleic Acid Symposium Series* **2008**, 52, 681-682.

[91] Zhang, D. Y.; Turberfield, A. J.; Yurke, B.; Winfree, E. Engineering Entropy-Driven Reactions and Networks Catalyzed by DNA. *Science* **2007**, 318, 1121-1125.

[92] Porchetta, A.; Ippodrino, R.; Marini, B.; Caruso, A.; Caccuri, F.; Ricci, F. Programmable Nucleic Acid Nanoswitches for the Rapid, Single-Step Detection of Antibodies in Bodily Fluids. *J. Am. Chem. Soc*. **2018**, 140, 947-953.

[93] Ranallo, S.; Prevost-Tremblay, C.; Idili, A.; Vallee-Belisle, A.; Ricci, F. Antibody-powered nucleic acid release using a DNA-based nanomachine. *Nat. Commun.* **2017**, 8, 15150.

[94] Ranallo, S.; Rossetti, M.; Plaxco, K. W.; Vallee-Belisle, A.; Ricci, F. A Modular, DNA-Based Beacon for Single-Step Fluorescence Detection of Antibodies and Other Proteins. *Angew. Chem. Int. Ed.* **2015**, 54, 13214-13218.

[95] Mahshid, S. S.; Camire, S.; Ricci, F.; Vallee-Belisle, A. A Highly Selective Electrochemical DNA-based Sensor that Employs Steric Hindrance Effects to Detect Protein Directly in Whole Blood. *J. Am. Chem. Soc.* **2015**, 137, 15596-15599.